Ricardo Naoyuki Alves de Moraes Sawaguchi

Development of an Electromechanical Actuator for Downhole Inflow Control Valves

Dissertação de Mestrado

Dissertation presented to the Programa de Pós-Graduação em Engenharia Mecânica of PUC-Rio in partial fulfillment of the requirements for the degree of Mestre em Engenharia Mecânica.

Advisor: Prof. Arthur Martins Barbosa Braga

Rio de Janeiro
May 2024

Ricardo Naoyuki Alves de Moraes Sawaguchi

Development of an Electromechanical Actuator for Downhole Inflow Control Valves

Dissertation presented to the Programa de Pós-Graduação em Engenharia Mecânica of PUC-Rio in partial fulfillment of the requirements for the degree of Mestre em Engenharia Mecânica. Approved by the Examination Committee.

Prof. Arthur Martins Barbosa Braga
Advisor
PUC-Rio

Prof. João Carlos Ribeiro Plácido
PUC-Rio

Dr. Giancarlo Vilela de Faria
Ouro Negro Tecnologias em Equipamentos Industriais S.A.

Dr. Roberth Waldo Angulo Llerena
Ouro Negro Tecnologias em Equipamentos Industriais S.A.

Rio de Janeiro, May 28th, 2024

Ricardo Naoyuki Alves de Moraes Sawaguchi

Has a degree as a mechanical technician, completed in 2015, and majored in mechanical engineering in 2020 both by CEFET/RJ. Seven-year experience with All-electric Intelligent Well Completion projects. Author and co-author of three patents filed. Mechanical design coordinator in the research and development project for the electric interval control valve and electric subsurface safety valve to be installed in the Brazilian Pre-salt wells at ouronova.

To my mother who supported me my whole
life and my beloved wife.

Acknowledgements

To my advisor, Professor Arthur Braga, who gave me invaluable support for this work to be completed and whom I admire for his entrepreneurial mindset.

A special thanks to Felipe Noel and ouronova that gave me this opportunity in this Research and Development journey seven years ago and allowed this work to be done and published.

Abstract

Sawaguchi, Ricardo Naoyuki Alves de Moraes; Braga, Arthur Martins Barbosa (Advisor). **Development of an Electromechanical Actuator for Downhole Inflow Control Valves.** Rio de Janeiro, 2024. 94p. Dissertação de Mestrado – Departamento de Engenharia Mecânica, Pontifícia Universidade Católica do Rio de Janeiro.

The seek for higher efficiency, reliable systems, and carbon footprint reduction is a trend in the Oil & Gas (O&G) industry. Intelligent Well Completion (IWC) has become a widely adopted and the Inflow/Interval Control Valve (ICV) plays a significant role in controlling production and injection flow rates. Electrification of O&G assets, including the IWC tools, offers a dual benefit of increased recovery factors and alignment with global decarbonization efforts. To develop an Electric ICV, the design of an electromechanical actuator capable of operating under challenging conditions and electrical power limitations is required. This dissertation presents the design and testing of an electromechanical actuator in a full-scale prototype Electric ICV. The actuator's performance was assessed through a combination of mathematical modeling and empirical testing under various operational conditions, including high and low temperatures and differential pressures. Key findings from this research demonstrated that the mathematical model effectively supported the actuator's design, with calculated results aligning closely with functional tests at room temperature and zero differential pressure.

Keywords

Well completion; Electromechanical actuator; Intelligent well completion; Downhole inflow control valve.

Resumo

Sawaguchi, Ricardo Naoyuki Alves de Moraes; Braga, Arthur Martins Barbosa (Orientador). **Desenvolvimento de um Atuador Eletromecânico para Válvulas de Controle de Fluxo de Fundo do Poço.** Rio de Janeiro, 2024. 94p. Dissertação de Mestrado – Departamento de Engenharia Mecânica, Pontifícia Universidade Católica do Rio de Janeiro.

A busca por maior eficiência, sistemas confiáveis e redução da pegada de carbono é uma tendência na indústria de Petróleo e Gás (O&G). A Completação Inteligente de Poços (IWC) tornou-se amplamente adotada, e a Válvula de Controle de Influxo/Intervalo (ICV) desempenha um papel significativo no controle da vazão de produção e injeção. A eletrificação dos ativos de O&G, incluindo as ferramentas de IWC, oferece um benefício duplo de aumento dos fatores de recuperação e alinhamento com os esforços globais de descarbonização. Para desenvolver uma ICV Elétrica, é necessário projetar um atuador eletromecânico capaz de operar sob condições desafiadoras e limitações de energia elétrica. Esta dissertação apresenta o projeto e os testes de um atuador eletromecânico em um protótipo de ICV Elétrica em escala real. O desempenho do atuador foi avaliado por meio de uma combinação de modelagem matemática e testes empíricos sob várias condições operacionais, incluindo alta e baixa temperaturas e pressões diferenciais. Os principais resultados desta pesquisa demonstraram que o modelo matemático apoiou efetivamente o design do atuador, com os resultados calculados alinhando-se com os testes funcionais em temperatura ambiente e pressão diferencial zero.

Palavras-chave

Completação de poços; Atuador eletromecânico, Completação inteligente de poços, Válvula de controle de fluxo de fundo do poço.

Table of contents

List of figures

List of tables

List of symbols and abbreviations

$B_{rb_{1,2}}$	Radial bearing's width $[mm]$
C_0	Basic load given by ISO 76 $[N]$
C_v	Flow coefficient $[m^3/h]$
D_{ab}	Axial bearing's outer diameter $[mm]$
D_{pw}	Distance between center of balls within axial bearing $[mm]$
$D_{rb_{1.2}}$	Radial bearing's outer diameter $[mm]$
D_{sl}	Sliding sleeve outer diameter $[mm]$
D_w	Axial bearing ball diameter $[mm]$
F_a	Actuation force $[N]$
F_{ab}	Axial force from pre-load spring acting on axial bearing $[N]$
F_{fcs}	Friction force of the closing seal $[N]$
$F_{fds_{1,2}}$	Friction force from dynamic seal #1 and #2 $[N]$
$F_{friction}$	Sum of the friction forces $[N]$
$F_{pl_{ab}}$	Force from the axial bearing's pre-load spring $[N]$
F_r	Radial force acting on bearing $[N]$
I	Electric current $[A]$
I_{in}	Input current $[mA]$
I_{in}	Input electrical current $[A]$
J	Second moment of mass $[kg \cdot m^2]$
J_{seal}	Geometry factor for V-ring seals $[mm]$
$M_{0_{ab}}$	Frictional torques as a function of speed for the axial bearing $[Nm]$
$M_{0_{rb_{1,2}}}$	Frictional torques as a function of speed for the radial bearings $[Nm]$
$M_{1_{ab}}$	Frictional torques as a function of load for the axial bearing $[Nm]$
$M_{1_{rb_{1,2}}}$	Frictional torques as a function of load for the radial bearings $[Nm]$
M_0	Frictional torque as a function of speed n < 2000 $[Nm]$
M_1	Frictional torque as a function of load for needle roller and cylindrical roller bearings $[Nm]$
M_R	Total frictional torque of bearings $[Nm]$
N	Number of rings in a V-Ring seal pack

$P_{e_{max}}$	Maximum electrical power [W]
P_1	Decisive load for axial ball bearings [N]
P_h	Mechanical actuator pitch [mm]
P_e	Electrical power [W]
P_m	Mechanical power [W]
S	Spring factor for V-ring seals [N/mm]
$T_{ab_{1,2}}$	Frictional torque from axial bearing #1 and #2 [Nm]
T_a	Ball screw actuation torque [Nm]
T_{emd}	Torque from the electromechanical device [Nm]
T_{fcs}	Friction force from valve`s closing seal [Nm]
$T_{friction}$	Sum of frictional torques [Nm]
T_{ma}	Frictional torque from mechanical actuator [Nm]
$T_{rb_{1.2}}$	Frictional torque from radial bearing #1 and #2 [Nm]
$T_{viscous}$	Frictional viscous torque [Nm]
V_{in}	Input voltage [V]
V_{max}	Maximum voltage [V]
W_{rp}	Mass of the rotating parts [kg]
Z	Number of balls within the axial bearing
b_v	Viscous coefficient of friction [$Nm \cdot s$]
d_M	Bearing's mean diameter [mm]
d_{ab}	Axial bearing's inner diameter [mm]
d_{ma}	Mechanical actuator's distance between balls at opposite sides [mm]
$d_{rb_{1.2}}$	Radial bearing's inner diameter [mm]
$f_{0_{ab}}$	Frictional torque bearing factor as a function of speed for the axial bearing
$f_{0_{rb}}$	Frictional torque bearing factor as a function of speed for the radial bearing
$f_{1_{ab}}$	Frictional torque bearing factor as a function of load for the axial bearing
$f_{1_{rb}}$	Frictional torque bearing factor as a function of load for the radial bearing
f_0	Frictional torque bearing factor as a function of speed
f_1	Frictional torque bearing factor as a function of load
$f_{PTFE_{PEEK}}$	Factor of rigidity between PTFE and PEEK rings
g	Gravitational acceleration (9,81 m/s^2)

k_t	Motor torque constant [Nm/s]
α	Angular acceleration [rad/s^2]
α_{ab}	Axial bearing load angle [°]
β	Mechanical actuator lead angle [°]
η_{em}	Electromechanical efficiency
η_{ma}	Mechanical actuator's efficiency
μ	Coefficient of friction
ω	Angular speed [rpm]
Δp_{cs}	Differential pressure acting on the closing seal [psi]
Δp_{ds}	Differential pressure acting on the dynamic seal [psi]

API	American Petroleum Institute
BOE	Barrel of oil equivalent (BOE)
BPD	Barrel per day
CAPEX	Capital Expenditure
CCUS	Carbon capture, utilization, and storage
CFD	Computational fluid dynamics
CONAMA	Conselho Nacional de Meio Ambiente
DC	Direct current
E&P	Exploration and Production
ERC	Extreme-reservoir-contact
FEA	Finite element analysis
FMECA	Failure Mode, Effect and Cause Analysis
FPSO	Floating, production, storage, and offloading
HMI	Human-machine interface
ICD	Interval Control device
ICV	Interval Control valve
IEA	International Energy Agency
IWIC	Intelligent Well Interface Card
MSE	Metal spring energized
NZE	Net zero emissions
O&G	Oil and Gas
OPEX	Operational Expenditure
OTA	Oil & Gas Authority
PCB	Printed circuit board

PEEK	Polyetheretherketone
PTFE	Polytetrafluoroethylene
R&D	Research and development
RCFA	Root cause failure analysis
RIH	Run in hole
SCSSV	Surface-controlled subsurface safety valve
SIT	System Integration Testing
SSV	Subsurface safety valve
TRC	Technology readiness categorization
TRL	Technology readiness level
UKCS	UK Continental Shelf
USD	United States dollar
WCT	Wet Christmas Tree
WDT	Wet Disconnect tool

1
Introduction

The constant research for higher efficiency and reliably systems and carbon footprint reduction are a reality for the Oil & Gas (O&G) industry. The Intelligent Well Completion (IWC) is a well completion method widely used with the former purpose as it increases the recovery factor from hydrocarbons reservoirs. Within the IWC, the inflow/interval control valve (ICV) may be considered as the heart of this system since it is the equipment directly used to control the flow production or injection.

Electrification of the assets in the O&G industry is a path not only to achieve an increased recovery factor, but also to the decarbonization efforts of this business sector aligned with the global net-zero commitment. For this purpose, an Electric ICV is necessary and the actuation method to open and close the valve needs to be designed to be able to work under the challenging operational conditions and electrical power limitations for the electric IWC. An electromechanical actuator is the strongest candidate for this task which low power consumption with high actuation forces can be achieved.

The objective of this dissertation is to present the design of an electromechanical actuator tested in a full-scale prototype Electric Interval Control Valve and compare the calculation results, from the adopted mathematical model, with the experimental data gathered from the tests.

Findings of this research allowed the full-scale Electric ICV's prototype to be concept-proven, achieving the Technology Readiness Level (TRL) 4 in a scale from 1 to 9.

This thesis is structured as follows: Chapter 2 presents a literature review concerning what is the electric intelligent well completion, its advantages compared to the conventional methods and relation to the decarbonization scenario through the electrification of the Oil & Gas industry, the Brazilian and international markets. Also, a review of the existing technologies for interval control valves and the development methodology for new downhole technologies; Chapter 3 outlines the methodology adopted in this work. The function, mathematical model, and calculation results of the designed electromechanical actuator taking into account a

planned laboratory test program are presented; Chapter 4 presents the experimental data obtained from the tests with the full-scale prototype during different ambient conditions such as high or low temperatures and differential pressures. These empirical data are compared to the calculated results to validate the mathematical model; Chapter 5 concludes the work summarizing the methodology, the relevance of the results comparison and suggestions for future improvements.

2
Literature Review

2.1
Electric Intelligent Well Completion

Well completion is the operation that takes place after drilling that aims to prepare the well for production. At this stage, a specialized hardware is placed in the borehole with the function of providing mechanical support and to regulate the fluid flow [1]. According to the authors, completions functions can be categorized as:

1.   Well integrity and fluids containment – completions are well barriers and must guarantee the well integrity throughout its life;

2.   Well/completion flow efficiency – maximize the flow production while being economical;

3.   Borehole and casing stability – the maintenance of the well mechanical stability must be assured by the type of completion tooling associated;

4.   Sand/solids control – sand production is unwanted as it may damage the tubing, valves and flowlines throughout the production system and completion tools shall work to prevent or allow and acceptable sand production;

5.   Selective/zonal flow control – production zones can be implemented in a completed wellbore to optimize oil/gas recovery and prevent unwanted fluid production, like water, to the surface with the assistance of sliding sleeves to selectively open/close a specific zone. Figure 2 shows an example of sliding sleeves combined with packers, for production zone delimitation, in different zones to prevent production of water by means of the sliding sleeve closure in the specific water producing zone.

Depending on the well parameters, there are several well completions configuration. Figure 1 shows the most common types of completions. In an open-hole completion, the hydrocarbon-fluid from the reservoir moves to a non-

horizontal producing interval. Slotted liner completion can be used to accelerate the fluid flow and this configuration can be used when the formation strengths are not enough. In cemented, cased, and perforated completions the flow from the reservoir approaches the wellbore in parallel streamlines which converges to the perforations. Gravel pack completions have a pack of gravel and along with a screen around the production tubing to prevent the production of unwanted sand.
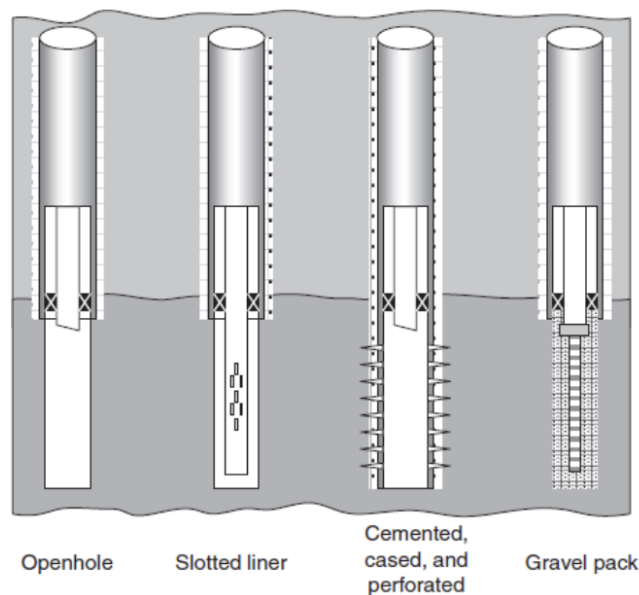
Figure 1: Most common types of well completion. Open hole; Slotted Liner; Cemented, cased, and perforated; and Gravel pack [1]
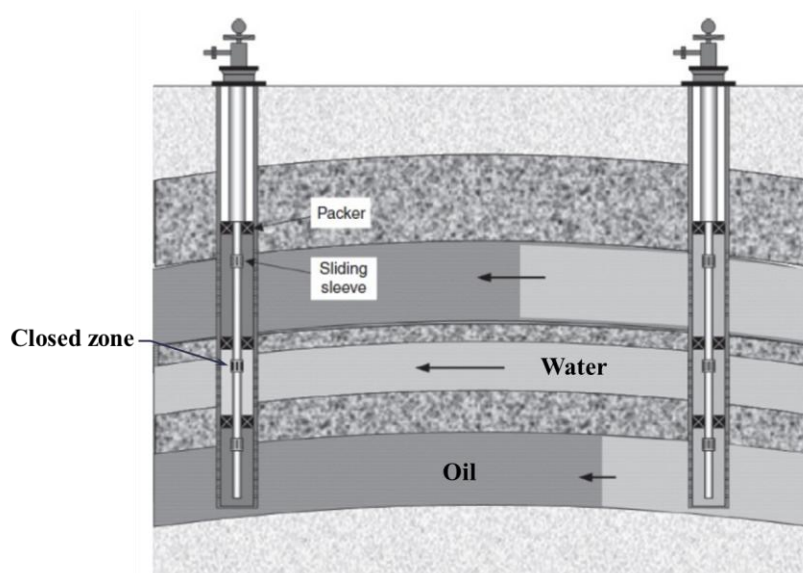
Figure 2: Sliding sleeves can be used to selectively close production zone where unwanted fluids, like water, is being produced. (Adapted from [1])

The well completion can be divided into upper completion, where the subsurface safety valve and tubing hanger are located, and lower completion, which connects the reservoir directly to the wellbore through packers, sliding sleeves and flow control devices [1].

In an IWC, there are three main types of well construction and completion with other types being variations of the following:

- Multi-zone/layered completion (Figure 3a) – this type of completion allows the commingled production and has the zones isolated from each other through packers and the flow production is controlled by ICVs installed in each zone;

- Sand control completion (Figure 3b) – depending on the reservoir formation characteristics, there is a need for control of the sand produced through gravel pack and/or screens. This type of completion can also be multi-zoned;

- Multi-lateral completion (Figure 3c) – to increase the contact area of the wellbore with the reservoir or reservoir's layers, lateral or branches can also be drilled and being controlled independently in each producing zone by its respective IWC components.
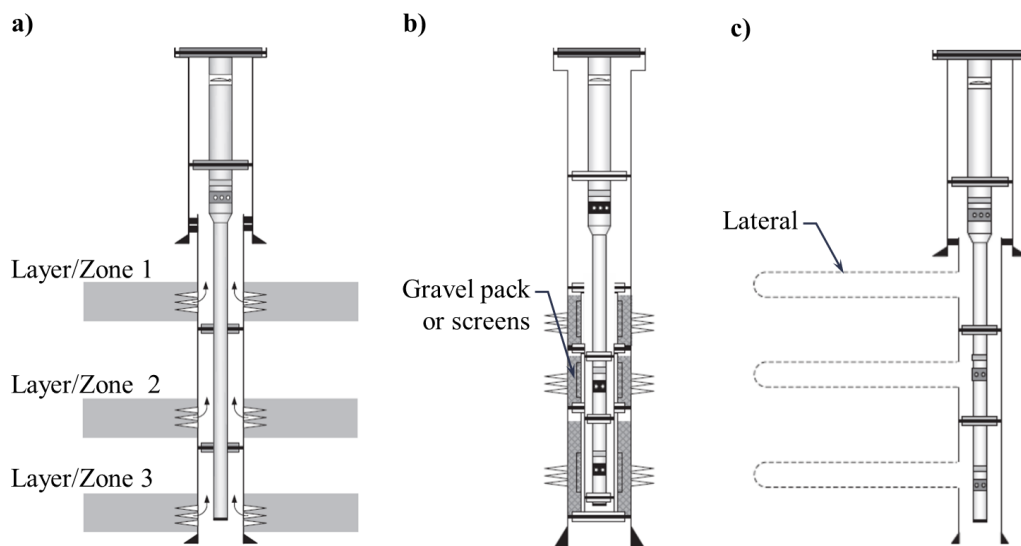
Figure 3: Main types of well completion. a) Multi-zone/layered completion. b) Sand control completion. c) Multi-lateral completion (adapted from [1]).

2.1.1

What is Intelligent Well Completion

Intelligent Well Completion (IWC) is a well completion technology which data from the completed wells are used to optimize the reservoir`s performance from producing and injector wells. The data is collected, processed, and analyzed through numerical or analytical models. Depending on the solution identified by the model to improve the hydrocarbon recovery, an action is taken in the field by controlling devices within the intelligent well, for example, the interval control valve (ICV). Devices such as permanent downhole gauge (PDG) and fiber optics sensing are used for acquiring data temperature, pressure, vibration. With the IWC, the operator can remotely monitor and control the well performance without physical intervention.

Intelligent well completion allows the production from commingled multiple zones with the implementation of interval control valves (ICV). This means removing the need for several wells to individually explore different layers and drilling only one well to control the production of from different layers, as shown in Figure 4. Another application of IWC is to control water flooding which can be done through the change of injection rates in different production zones by the respective ICVs. Reducing the water produced to the surface, reduces the cost of processing the fluids from the well. Another benefit from the IWC is that the operator can monitor the mechanical integrity and environmental conditions of the wellbore and modify the operating conditions to keep them within an acceptable integrity operating envelope [2].
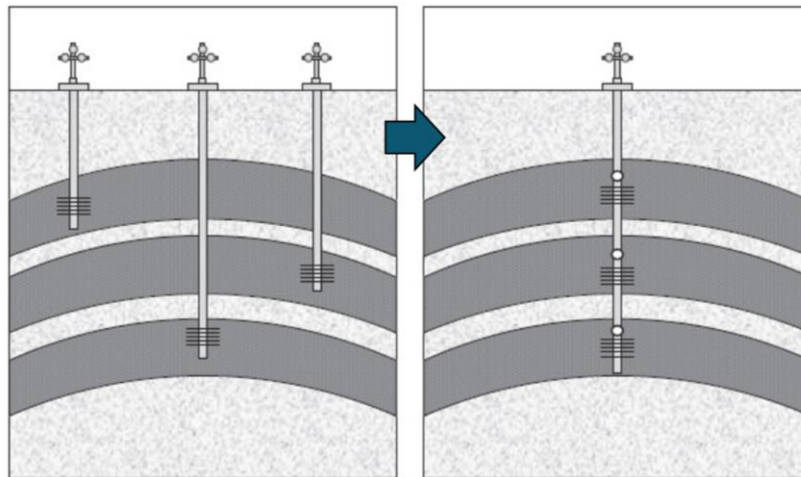
Figure 4: Multiple layers for production with conventional well completion for each layer to single commingled intelligent well completion (adapted from [1])

Summarized by [3], the benefits of the IWC are:

• Commingling Feasibility: Adjusting the downhole pressure differential enables commingling across various reservoir layers;

• Crossflow Elimination: Optimizing production through reduced frictional losses;

• Coning Control: Selective pressure reduction at strategic reservoir points can manage water and gas coning (Figure 5);

• Production Optimization: Modifying choke settings can optimize oil output while controlling the gas-oil relation and water-cut increases over time;

• Injection Rates Regulation: adjusting water or gas injection rates for specific well sections enhances sweep efficiency and production.
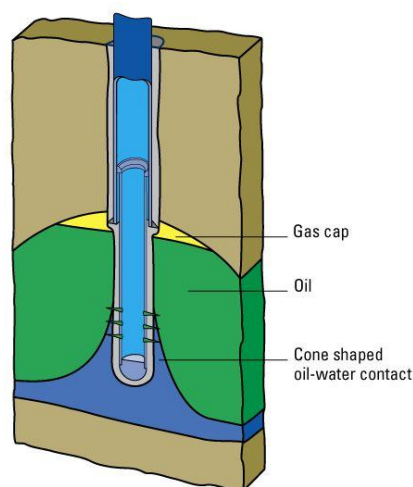
Figure 5: Water coning [4].

Within the IWC, there are some equipment commonly installed in the lower completion. They are listed below with their functions:

- Interval control valve (ICV) – control the flow rate of a zone in a producing or injecting well, depending on the application. This control can be done through hydraulic, electrohydraulic, or electric actuation systems. Figure 6a show an example of a multi-position ICV;

- Permanent downhole gauge (PDG) – usually a pressure and temperature sensor installed within the tool (PDG) to measure these parameters in a specific zone. Other sensors can be used, less commonly, like vibration. Fiber-optics sensing can also be used. Figure 6b shows a schematic drawing of a PDG mandrel with its main components.

- Zonal isolation packer –equipment used to seal the zones in a multi-zone/commingled well. Figure 6c shows a production packer with its main components.

a)

b)   c)
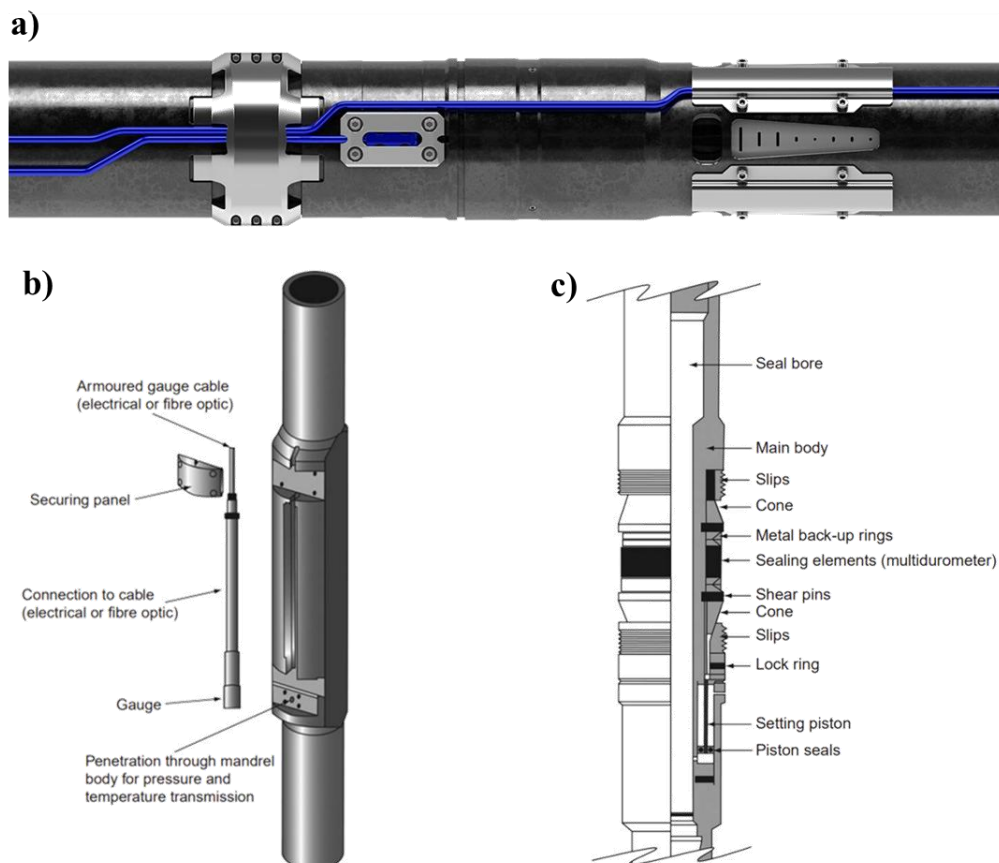
Figure 6: Main equipment commonly installed in the intelligent well completion (lower completion). a) Interval control valve [5]. b) Permanent downhole gauge (PDG) components [6]. c) Production packer components [6]

As for the upper completion, the main components and functions are:

• Subsurface Safety Valve (SSV) – it is a valve with a fail-safe system that allow the valve to close immediately in an emergency preventing the uncontrolled release of hydrocarbons to the surface. In Figure 7a, the SSV is shown with its key components;

• Gas-lift valve – optional and used when it is predicted the need for artificial lift methods with gas injection to reduce the produced fluid density and increase the oil recovery. Figure 7b shows a gas lift valve installed in a side pocket mandrel.

• Wet disconnect tool (WDT) – tool used to connect and disconnect the upper completion from the lower completion allowing the removal of the components from the upper portion without interfering with the lower ones.
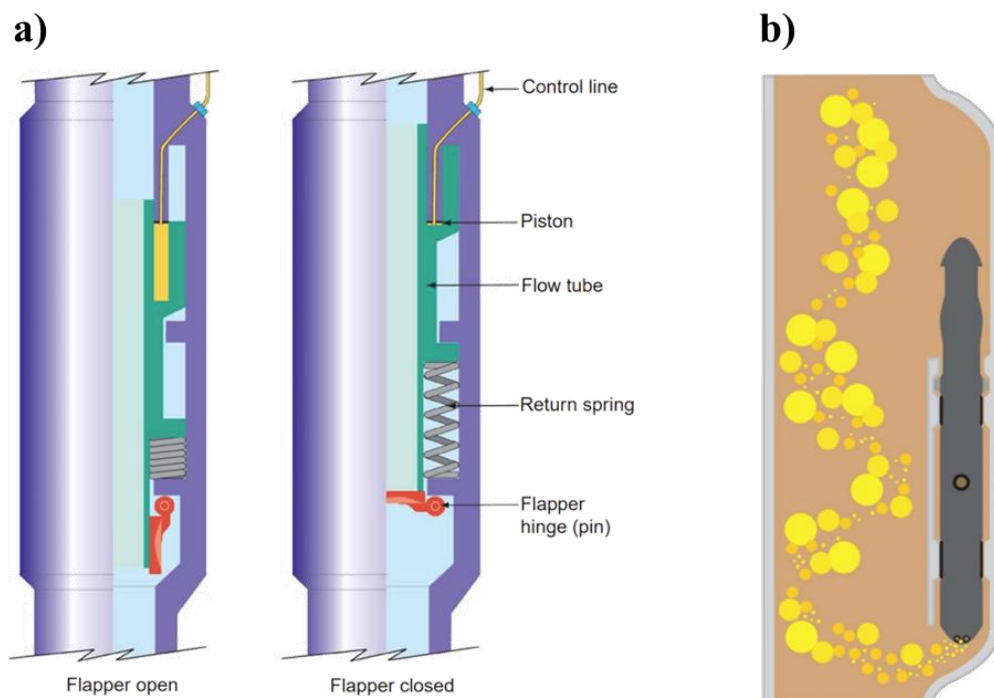
Figure 7: Some of the tools installed in the upper completion. a) Subsurface Safety Valve (SSV) [6]. b) Gas lift valve in a side pocket mandrel [6].

2.1.2

Decarbonization, Electrification, and the All-Electric Intelligent Well Completion

Towards the global net-zero commitments, electrification and renewable energies have the highest interest score and had more than $ 250 billion of investments in 2022 as noted in a report of technologies trends in 2023 from McKinsey & Company [7]. Although the innovation score, which accounts for new patents and research, is not as high as "Applied AI," electrification and renewables has also the fourth highest innovation score, as shown in Figure 8.
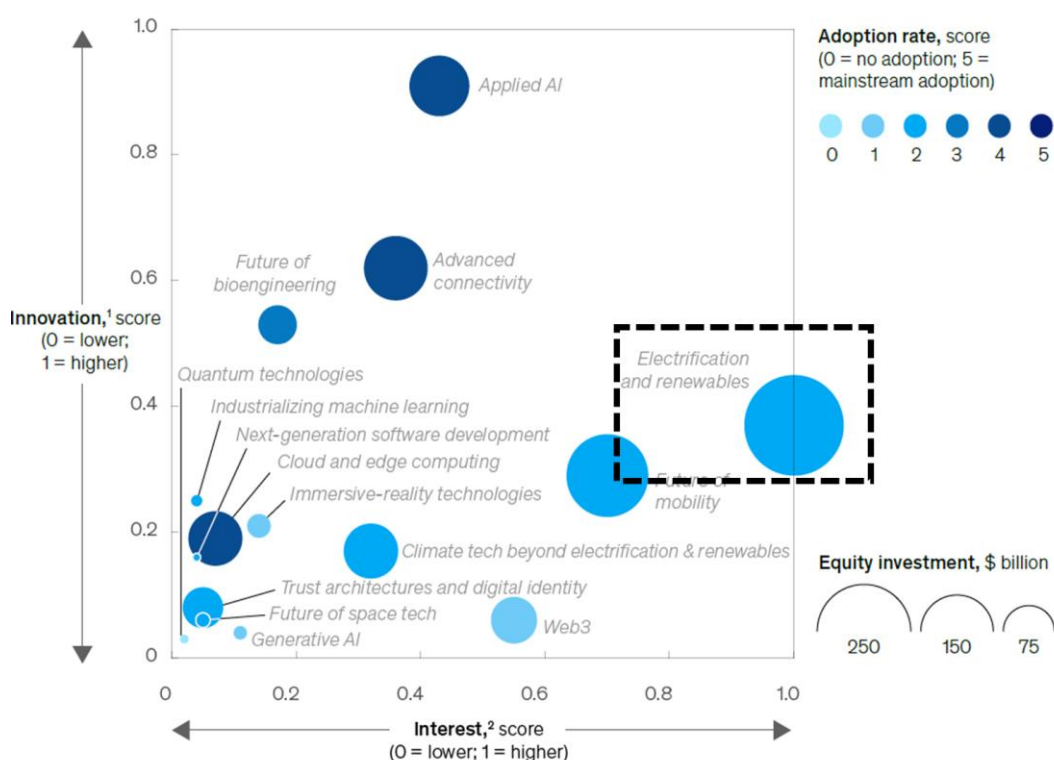
Figure 8: Technologies trends in 2023: Electrification and Renewable Technologies has the highest score along with the highest investment in 2022 (Adapted from [7])

The total share of global emissions in 2015 from the oil and gas industry was 42%, from direct (8%) and indirect (1%) operations and from the sector`s value chain (33%) [8]. As also highlighted by [8], several decarbonization technologies can help reduce the total CO_2 emissions of the industry, as shown in Figure 9. The "Extraction and drilling" segment, which is part of the upstream category and includes the well completion, has an emission share of 10% which can be reduced by electrification technologies. The All-Electric Intelligent Completion can play a significant role in this transition.
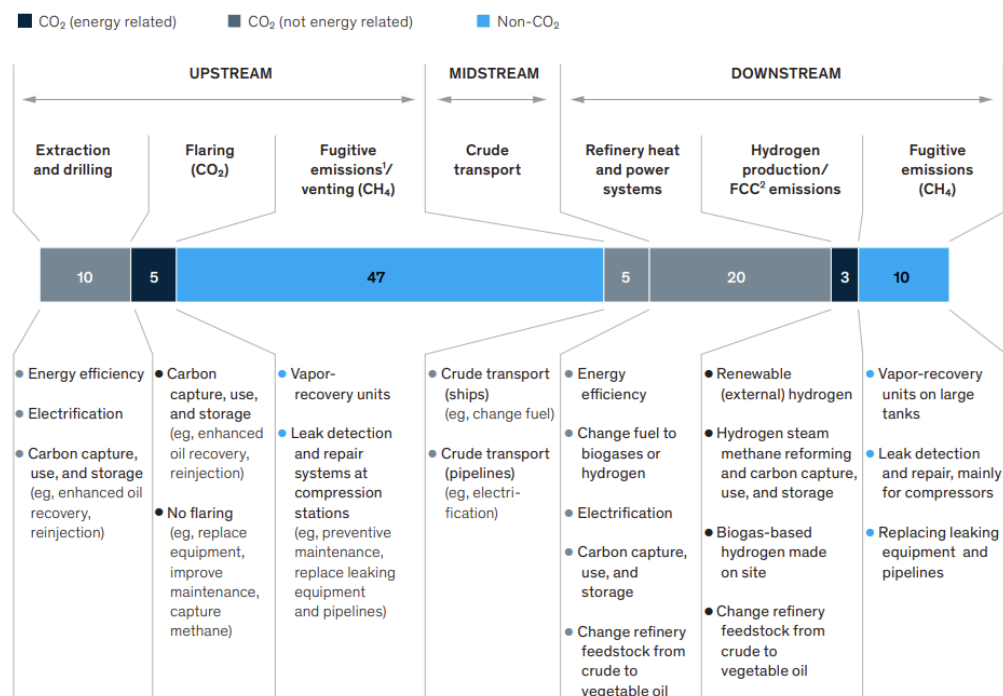
Figure 9: Percentage of CO2 emissions by source and possible solutions within the oil and gas industry. [8]

The International Energy Agency (IEA) published a report in 2023 [9] describing a Net Zero Emission (NZE) scenario by 2030 which the upstream sector could reduce, starting in 2022, 70% for oil and 60% for gas operations, as shown in Figure 10a. Some key drivers for emissions reduction were highlighted (Figure 10b): reduction in demand, tackling methane emissions, eliminate all non-emergency flaring, electrification of upstream facilities, carbon capture utilization and storage (CCUS) equipment implementation in the oil and gas processes and increase of low-emissions electrolysis hydrogen in the refining process.
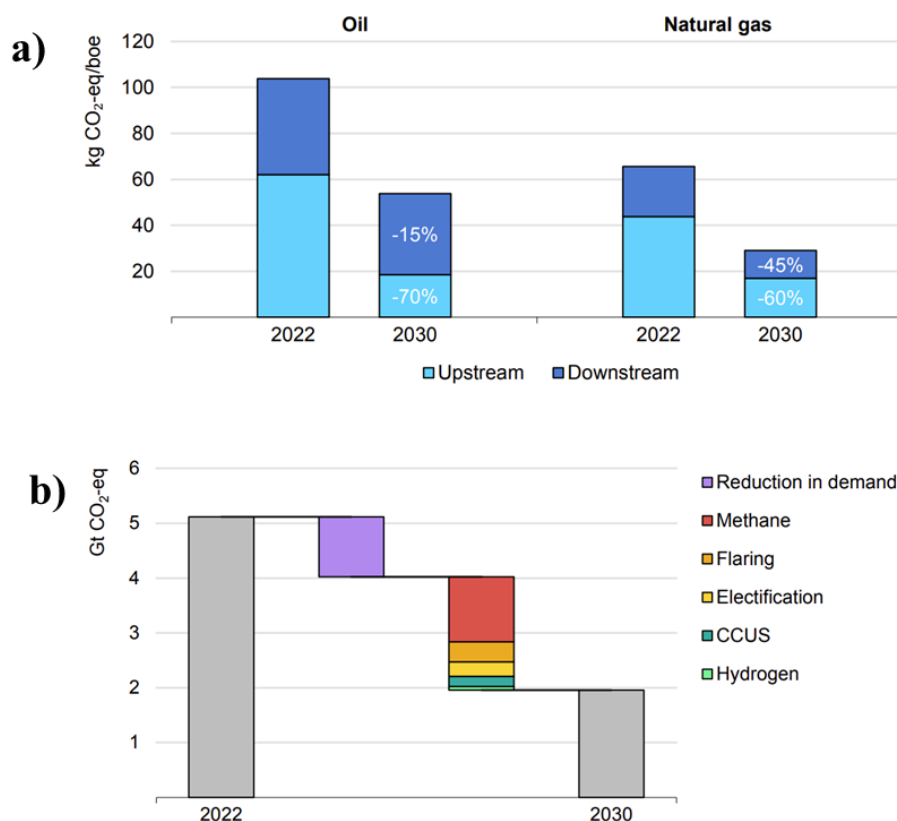
Figure 10: Reduction of CO2 emissions in the oil and gas industry by 2030 in the Net Zero Emissions scenario from IEA's 2023 report. a) Summary of reductions for oil and gas in the upstream and downstream segment. b) Reductions by key drivers. [9]

In the United Kingdom, as reported in 2020 [10] by the Oil & Gas Authority (OTA), the electrification of offshore structures, new (greenfields) or existing (brownfields), is a reality for the commitment of their Oil & Gas (O&G) sector that can even potentialize the use of renewables as windfarms. As mentioned in the report, 70% of the offshore CO_2 emissions from the UK Continental Shelf (UKCS) facilities are due to power generation, which requires gas turbines today (Figure 11a). The electrification of theses offshore structures can be done with electricity coming from the onshore grid or offshore windfarms, or a mix of both, as shown in Figure 11b).

a)

b)
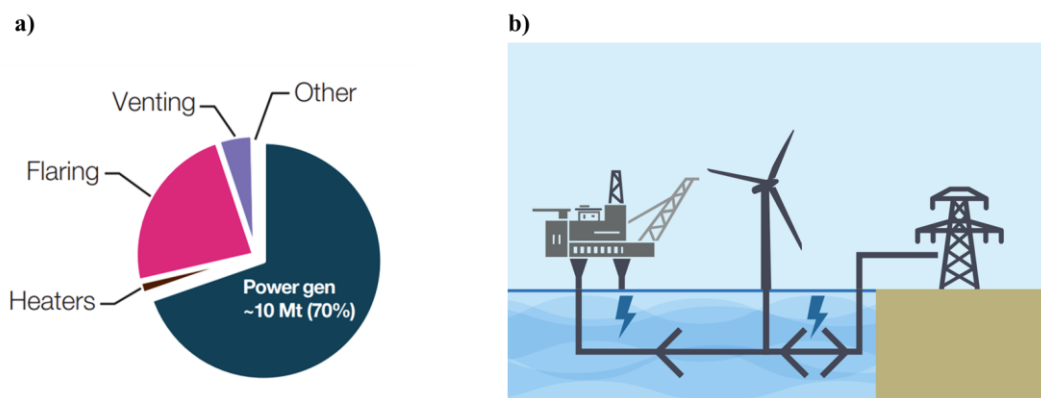
Figure 11: a) 70% of the UKCS CO_2 emissions are related to power generations for offshore platforms. b) Ways for partially or fully offshore electrification are obtaining power supply from can come from the onshore grid or offshore windfarms [10]

2.1.3

Advantages of the Electric Intelligent Well Completion (Wells Electrification)

The Electric IWC is related to the electrification of offshore facilities as the Oil & Gas (O&G) industry is aligned with the 2050 Net Zero commitment. As these structures are partially or completely electrified, the entire system should be electric so it can have the most effectiveness. Not only this, the Electric IWC allows for the optimization of control of the IWC components like ICV and sensors since with only electric cable it is possible to monitor and control multiple zones of commingled wells. Also, this is particularly important for deepwater wells, with the water layer as big as 3000 m [10,000 ft] where the conventional completion hydraulically actuated faces one of its biggest challenges due to the high hydrostatic pressure within the control lines.

As highlighted by [11], all three (hydraulic, electrohydraulic, and electric) IWC systems present advantages and disadvantages as shown in Table 1.

Table 1: Advantages and disadvantages between hydraulic, electrohydraulic, and electric IWC [11]

Hydraulic	
Advantages	Has a long time of field history with well-known possible issues and solutions
	ICVs are cheaper since there is less technology involved
	Has a high shifting force from hydraulic pressure
Disadvantages	Limitation of ICVs' installation depth
	Number of zones in a single wellbore is limited by the space available for the bypass of the hydraulic control lines in the Tubing Hanger
	Hydraulic fluid degradation, contamination, and leakage across the control lines
Electrohydraulic	
Advantages	Shifting forces are the same as hydraulic systems
	ICVs has the capability of providing data through the electric control lines
	Allows the installation of several ICVs in a single well with only two hydraulic lines and two electric lines
	Allow the choking in infinite positions
Disadvantages	Limitation of ICVs' installation depth
	Number of zones in a single wellbore is limited by the space available for the bypass of the hydraulic control lines in the Tubing Hanger
	Hydraulic fluid degradation, contamination, and leakage across the control lines
	Costs of the completion tools are higher than hydraulic systems
Electric	
Advantages	No limitation of installation depth of flow control valves imposed by actuation mechanism
	No concern about high operating pressures of flow control valves imposed by actuation mechanism
	Only one hole in the Tubing Hanger is needed to operate several ICVs and sensing tools
	No concern about fluid degradation, contamination; and leakage in control lines
	Installation depth is not limited by hydrostatic pressure in the control line
	Allow the installation of P&T, position, vibration sensors in a single ICV
	More space to bypass control lines for chemical injection
	Technology aligned with the decarbonization of the O&G industry
	Allow the choking in infinite positions
	Technology needed to allow IWC in three or more zones for deepwater wells
	Real-time data from ICV position, pressure and temperature, vibration is possible
Disadvantages	Excessive costs of the completion tools
	Reliability for long term usage still need to be proven
	Less field history than hydraulic and electrohydraulic systems
	Shifting forces limited by the electrical power available from the surface

2.1.3.1

Paths for Electrification of Intelligent Well Completions

In the oil and gas industry, the electrification can be understood as a conversion from hydraulic power and control systems to electric. To measure an oil field or asset performance, the carbon emissions per barrel of oil equivalent (BOE) has become another industry benchmark alongside with the cost per barrel. Then, the electrification of oil and gas operations plays a significant role in the decarbonization of the industry. As highlighted by Hiron S. and Edmundson S. [12], moving to electric technologies requires the adoption of integrated solutions at scale to allow for sustainable and efficient oil and gas operations. They described two steps to reach such a goal:

• Step 1: Access low-carbon power through adoption of electric high-power equipment which energy sources can come, for offshore facilities, from onshore grid or locally by offshore wind farms, Figure 12 shows the connections between a few platforms from the Norwegian company Equinor to a floating wind farm. Onshore facilities can be power supplied by low-carbon grid source or renewable ones. Minimizing energy consumption in oil and gas facilities is also needed as other sectors will also need low-carbon energy sources. This means that energy efficiency plays a key role for the oil and gas industry electrification to be worth it.

• Step 2: Implement fully electric production systems to maximize efficiency. The hydraulic systems conversion to electric ones enables the extended reach of wells as the first have limitation due to pressure drop caused by frictional losses in the control lines and requires a high number of connections, pump motors and big generators for equipment actuation. The electric-powered system allows for operation and data acquisition through much longer distances at an instant response along with enabling the digitalization of wells and other oil and gas facilities. These characteristics, within the completion approach, allows for multiple interval control valves (ICV) to be installed in discrete production zones of a well which maximizes the oilfield performance through minimizing water production. This can potentially reduce the need for more drilled wells to reach the targeted oilfield

performance, hence, reducing the carbon footprint of drilling and completion operations.

Figure 12: Connections between platforms, from the biggest Norwegian operator, Equinor, and a [13] floating windfarm for the electrification of these facilities [14]

At the subsea level, big oil companies like Total and Equinor are moving to the electrification of their subsea assets, existing and new ones, which will not only reduce the carbon footprint form exploration and production but will also reduce the capital expenditure (CAPEX) and operational expenditure (OPEX). Removing hydraulic control lines from the subsea system reduces the sizes of subsea umbilical along with the complexity of the control systems and design simplification of wet Christmas tree (WCT) and manifolds [15]. Another benefit of removing the hydraulic system is the elimination of hydraulic power units utilized to provide high pressure for the control system. Also, the fluid leakage has an environmental impact as leakages across the lines are common, which, for example, in a forty well field 150 liters of hydraulic fluid are consumed per day that also means an annual operational cost ranging from USD 500k to USD 2M. The electrification of all subsea structures like WCT, manifolds, control valves is a great ally to the all-electric intelligent well completion.

Another example of the electrification in the O&G industry is the partial electrification of a floating, production, storage, and offloading (FPSO) vessel, example shown in Figure 13a, that will operate in the Brazilian Pre-Salt. The main gas-fueled turbines (Figure 13b) that provided the mechanical loads were replaced by electric motors, with the limitation of generating power of up to 100 MW due to

a regulation from *Conselho Nacional de Meio Ambiente* (CONAMA) and the total load required for the FPSO to work properly required the maintenance of some gas turbines [16].
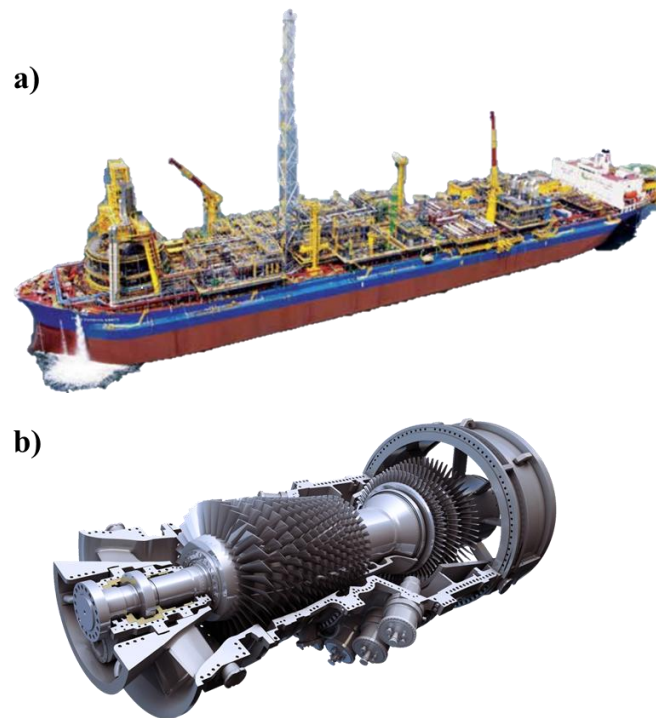
Figure 13: a) FPSO Espírito Santo (adapted from [17]). b) Example of gas turbine [18].

2.1.4
Electric Intelligent Well Completion Market in Brazilian and International Wells

Since 2000s, the biggest Brazilian oil company, Petrobras, recognizes the Brazilian Pre-Salt wells as candidates from the All-Electric IWC. Figure 14 shows the called Brazilian Pre-Salt polygon which extends from the Santos Basin to the Campos Basin covering 800 km of length and 200 km of width across the states of São Paulo, Rio de Janeiro, and Espírito Santo and the distance from the surface to the seabed can reach 3000 m of water depth. Petrobras is allowed to perform Exploration and Production (E&P) activities in 16% of the area, therefore 23.800 km^2, which they have been doing by means of consortia with other oil companies like Shell, Total Energies, Galp/Petrogal, Petronas, Repsol Sinopec, CNOOC and CNODC [19].
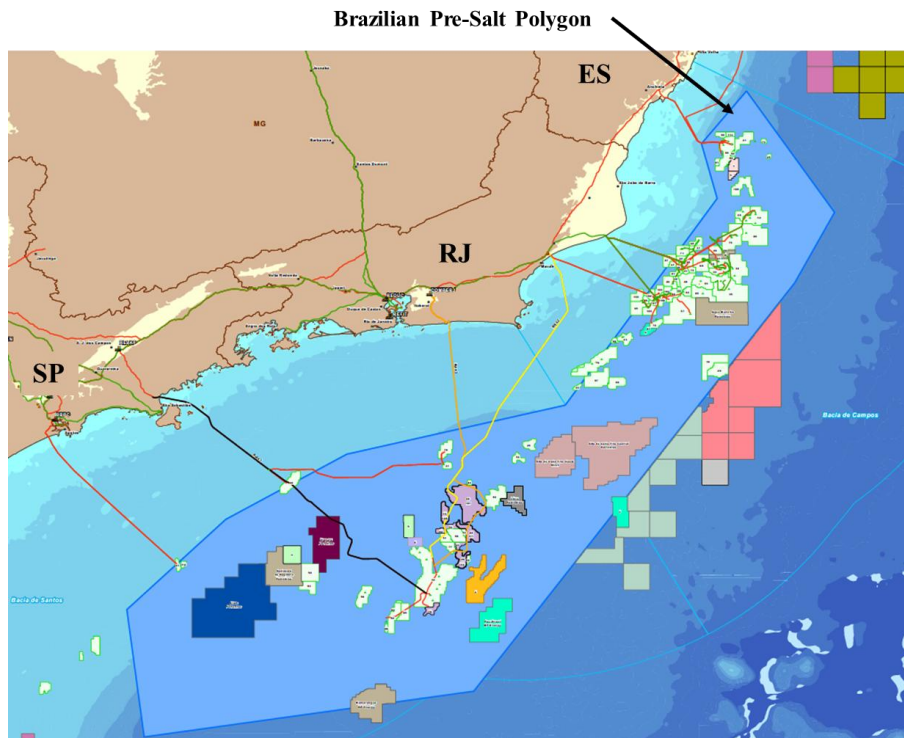
Figure 14: Brazilian Pre-Salt polygon: Santos and Campos basins locations across the states of São Paulo, Rio de Janeiro and Espírito Santo, and oil fields (Adapted from [20])

In August 2003 was installed the world's first all-electric well with IWC in an offshore well (8- MLS-67HA-RJS), 1180 m deep in the water, located in the Brazilian Pre-Salt's Marlim Sul field, Campos Basin. This installation was conducted by Baker Oil Tools and Petrobras in an initiative from the latter to enable IWC in water depths exceeding 3000 m [21]. In the recent years, the production of individual wells is becoming more relevant in the Pre-Salt with IWC technology, as observed by [22]. Fewer wells are planned with the aim to increase their productivity. IWC of multi-zone, multilateral and multi-zone, with three or more intervals, coupled with multilateral are options for the well construction. Also, faster response of ICVs, data monitoring and less space used by control lines for ICVs that allows the implementation of chemical injection valves are desired, so the best solution would be an Electric IWC which the reliability must be assured to be economical interesting. As of today, the Pre-Salt consortium has deployed over 100 wells with IWC technology which, soon, after service providers overcome the technological challenges required by newer technical specifications, the electric IWC can be fully adopted in new wells in Santos Basin fields [23].

Figure 15 shows a typical architecture of a 3-zones well with electric IWC to be installed in the Brazilian Pre-Salt wells. The platform is in the topside where the human-interface machine (HMI) where the operator monitors and controls the well. The umbilical (Figure 16a) is connected to the Vertical Connection Module (VCM), then the subsea lines are connected to the Wet Christmas Tree (WCT), Figure 16b. The IWC starts in the Subsea Control Module (SCM), Figure 16c, where the Intelligent Well Interface Cards (IWIC) are located. These cards are responsible for communication and control from the topside and power supply to the completion system. For the upper and lower completion, there are individual dedicated SCMs. Only one electric control line is necessary to operate and monitor the for each upper and lower completion electric tools. In the illustration, two holes are needed in the tubing hanger (Figure 16d) for the electrical control lines bypass. For the connection between the upper and lower completion, a Wet Disconnect Tool (WDT) is used, and feedthrough packers are utilized for isolation between productions zones/intervals.
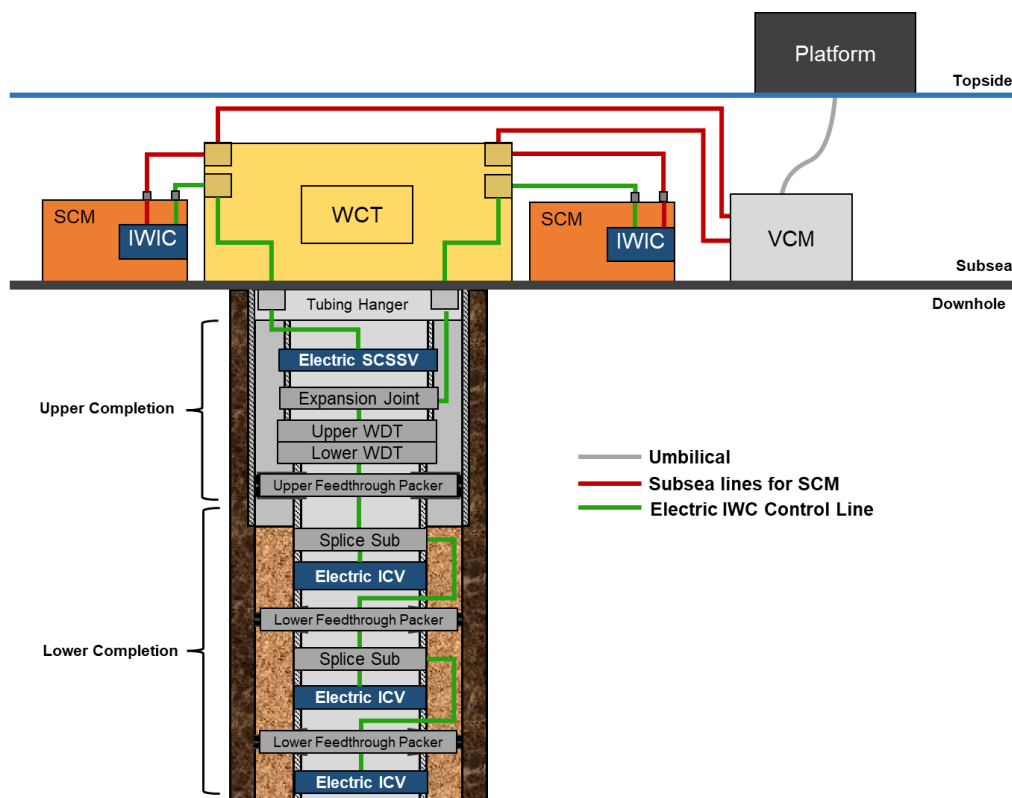
Figure 15: Typical architecture of a 3-zones Electric Intelligent Well for the Brazilian Pre-Salt [24]

a) b)

c) d)
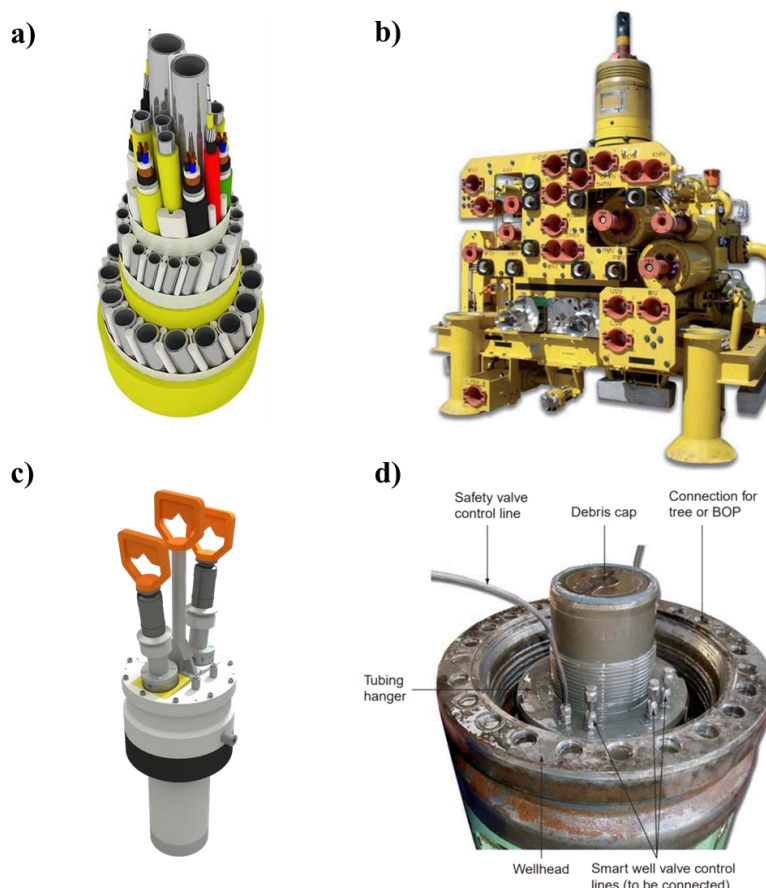
Figure 16: a) Example of umbilical with electrical lines, fiber optics, and steel tubes for hydraulic control and chemical injection [25]. b) Wet Christmas Tree (WCT) [6]. c). Subsea control module [26] d) Tubing hanger installed in the wellhead and control lines connections [6].

Following the developments of recent technology for Electric IWC in a search for cost-effective systems with ability for real-time monitoring, flow production control and data transmission, a new type of electric ICV was developed and field tested in China oilfields. For more than 15 months installed, the system did not present any issue and allowed to reduce the water cut, increased of production rate in a single well and increased the natural energy from the producing layer improving the reservoir recovery [27].

Offshore oil fields located in East Malaysia implemented the conventional hydraulic IWC in 2015 to optimize the oil recovery and in an effort for intervention-less solutions [28]. Later, in 2019-2020, the All-Electric IWC was installed in 4 out of 8 wells with significant early benefits identified like: up to 75% less installation time per zone, decrease of ICV's shifting time from hours, with hydraulic ICVs, to less than 5 minutes, with electric ones, and the need of only one electric control line

to install all completed production zones, which led to a cost savings of USD 600k for four wells installation.

In Saudi Arabia, tests with a prototype all-electric ICV for an IWC to be used in wells with reservoir that exceeds 10 km, known as extreme-reservoir-contact (ERC), were conducted for a year after well completion in January 2012 [29]. Two electric ICVs with printed circuit board (PCB) electronics, along with three hydraulic ICVs for reservoir management's risk mitigation, were installed in a multilateral well called "Well Trial No. 2". The electric tool had the capability to measure pressure, temperature, flow rates (Venturi meter) and water cut within the interval using a single electrical control line with twisted-pair conductors. The electric valve had the main objective of controlling the flow rate from zero to 1.500 BPD instead of the choking position.

Another application of an all-electric IWC in Saudi Arabia wells was an 8-zone system with an electric ICV that allows the installation of twenty-seven intervals with a single electrical control line and had six choking positions. Five electric ICVs were installed in an open-hole section of the well and three in a cased-hole portion to evaluate the application of the technology in both well scenarios. Hydraulic ICVs were installed for redundancy to assure a well productivity of 85% in case of failure of the electric ones. Also, installation and function testing were significantly less when compared to the conventional hydraulic ICV [30].

2.2
The Interval Control Valve (ICV)

The Interval Control Valve (ICV) may be considered the heart of the IWC. It is a component used to regulate the annulus to tubing flow rate in a specific production zone. The ICV's usually has a sliding sleeve which can be shifted powered by hydraulically, electro-hydraulically or electrically, remotely controlled from the surface (topside) with hydraulic and/or electrical control lines. Mechanical shifting through an intervention operation can also be used to move the sliding sleeve to a certain position when the primary actuation mechanism is lost due to failure. Usually, the way the ICV is powered dictates the IWC system being utilized. The following sections will describe the functioning, advantages, and limitations of each of the three existing systems.

2.2.1
Hydraulic ICV

Hydraulic ICVs are the most common valves used in IWC systems. Their actuation mechanism is relatively simple when compared to electrohydraulic and electric. As this technology is used by the industry for over 20 years, the reliability for long term usage of hydraulic valves is proven.

Differential pressure needs to be applied to a piston to shift a sliding sleeve to the open, closed, or intermediate position of the valve. The pressure on the piston area needs to provide enough force to overcome friction from the seals and eventual debris/deposits. To open the valve, a hydraulic fluid is pumped to the valve location in a control line connected to its chamber which will be filled to displace the sliding sleeve to the desired opening position. Whilst the valve is opening, hydraulic fluid is displaced back to the surface through the close control line. Closing the valve follows the same principle, but the fluid is pumped through the close control line instead. When the valve is open, the hydrocarbons migrate from the annulus region to the tubing through the flow ports which geometry can vary depending on the well application and can be an on-off or multi-position type. The former concept allows the valve to be either fully open or fully closed while the latter has intermediate open positions, discretized as necessary depending on application. Seals are used to prevent any leakage between the chambers and to guarantee the zero-flow rate through the interval. Figure 17 show a hydraulic ICV in the open and closed position with its main components.
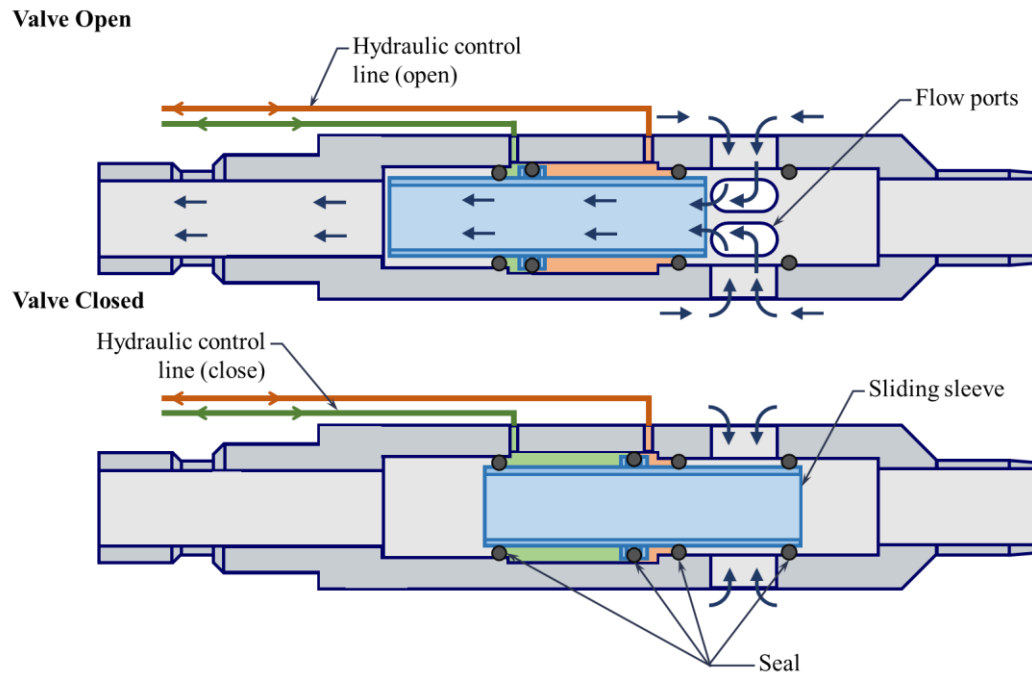
Figure 17: Hydraulic ICV in open and closed position with main components (Author)

In Figure 18 a 3-zone well section schematics with hydraulic ICVs is shown. The hydraulic IWC can have two control lines for each ICV (Figure 18a) or a called N+1 type which used one common close control line and one opening control line for each valve (Figure 18b). For both configurations, the number of valves within the IWC is limited by the installation depth and space available in the tubing hanger for control lines bypass but the N+1 is optimized in that matter.
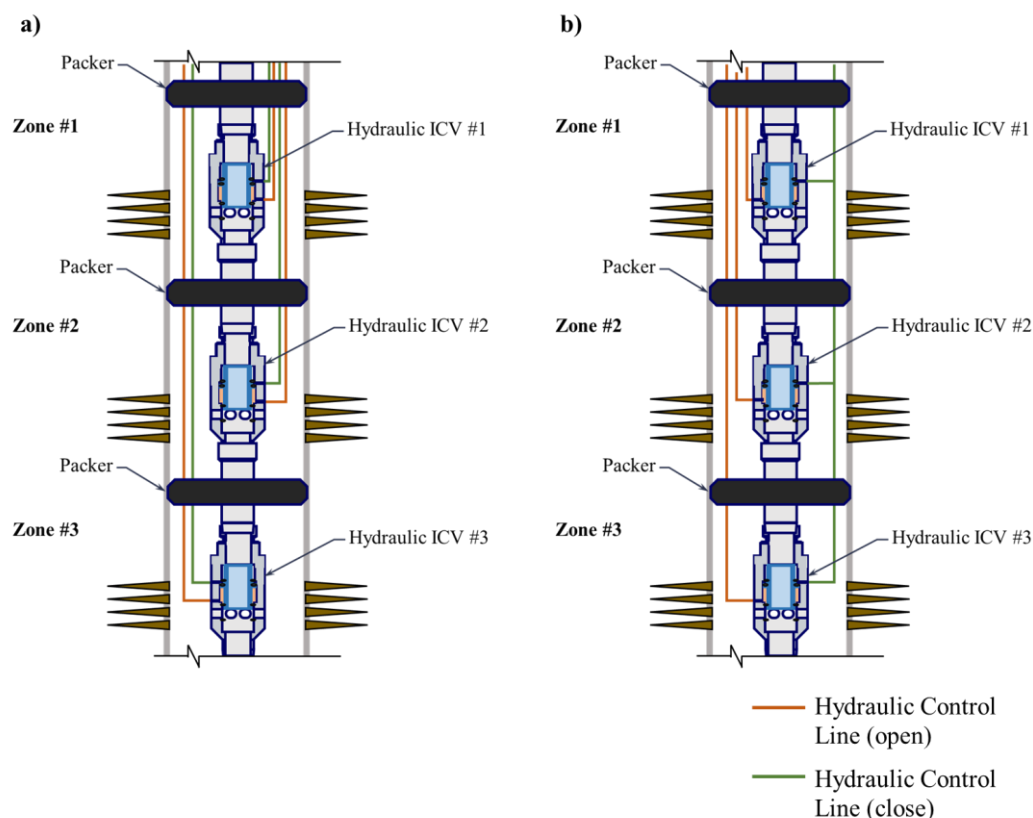
Figure 18: Well section schematic of a 3-zones hydraulic IWC with one hydraulic ICV per interval and packers separating each zone. a) Two hydraulic control lines are used for each ICV (open and close). b) One common close hydraulic control line (N+1 type) is used and one hydraulic control line for each valve for opening (Author)

2.2.2

Electrohydraulic ICV

Electrohydraulic ICVs have a device powered by electricity to divert the hydraulic fluid to the open or close chambers of multiple valves. Usually, a solenoid valve is used to perform this task. The open and close valve hydraulic control lines are still used but they are common for subsequent ICVs of other intervals. A command from the surface must be sent to the electric device to allow the opening of only one or more valves to be opened within the IWC. The electrical control line can also be used within the IWC for PDGs with pressure, temperature, flow rate and water cut sensors. Sliding sleeve's shifting time and force are still driven by the hydraulic fluid displacement from the surface until the ICV that needs its position changed. Another advantage of the electrohydraulic IWC is that by using common open and common close control lines, only three control lines bypass in the tubing hanger (two for hydraulic and one for the electric) are necessary for several valves. This leaves more room for the safety valve and chemical injection control lines,

giving more flexibility for production optimization. Figure 19 shows the main components of an electrohydraulic ICV in open and closed positions.
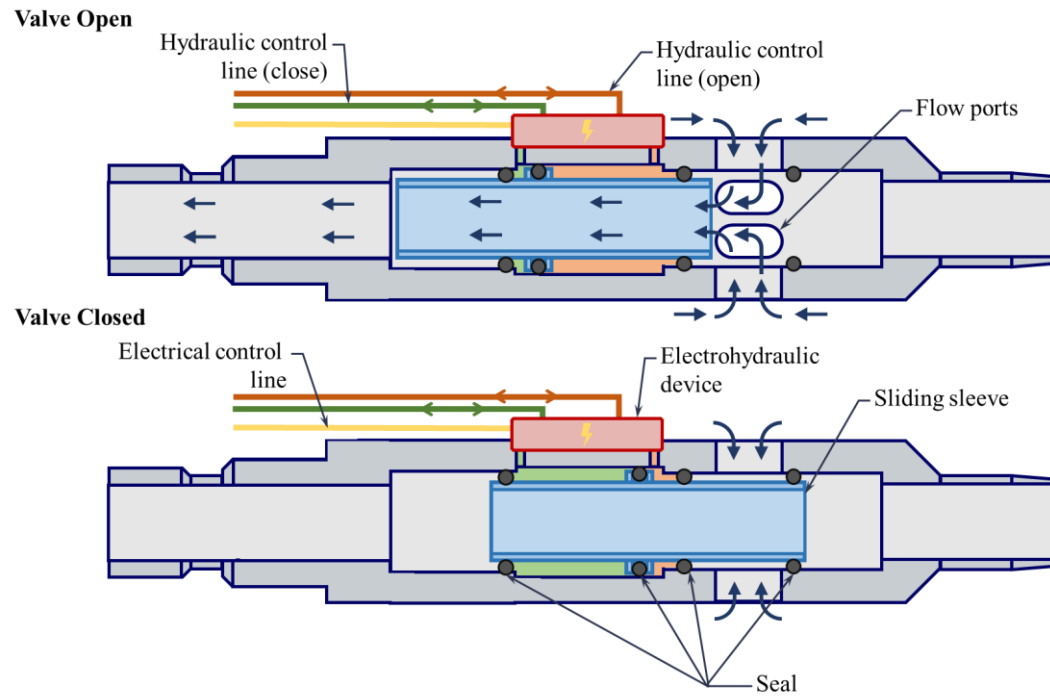
Figure 19: Electrohydraulic ICV in open and closed position with main components (Author)

Figure 20 illustrates three electrohydraulic ICVs in a 3-zones intelligent well. This figure also shows that that only three control lines (two hydraulics and one electric) are necessary to operate the three valves simultaneously or independently.
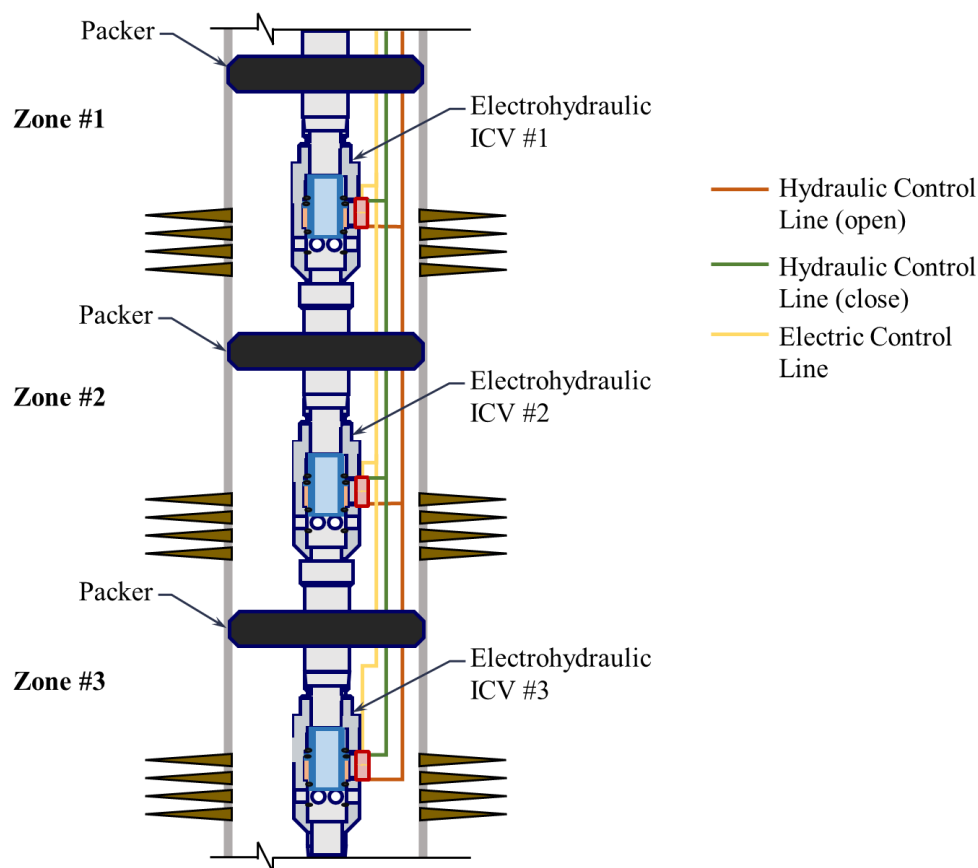
Figure 20: Well section schematic of a 3-zones electrohydraulic IWC with one electrohydraulic ICV per interval, packers separating each zone and two hydraulic control lines (common open and common close) and one electrical control line (Author)

2.2.3

Electric ICV

The all-electric IWC is still a technology that needs more adoption in the industry by proving its reliability through validation tests and time. However, besides being aligned with the decarbonization of the O&G industry by the electrification of all its assets, there are several benefits which an electric ICV brings to the IWC. They are listed below:

- One single electric control line can control multiple ICVs;

- The sliding sleeve position can be precisely measured by displacement sensors giving the choking position of an on-off, multi-position or infinite position valve in real-time;

- Shifting the valve from one position to another can take only a few minutes when hydraulic or electrohydraulic valves can take even hours;

- Sensors like pressure, temperature, flow rate, water cut, and vibration can be integrated in the IWC by that same control line;

- More space is left available for the subsurface safety valve and chemical injection control lines bypass in the tubing hanger;

- Number of production zones and maximum depth of the well are not limited by the hydrostatic pressure in the control line;

- Installation time of electric IWC is considerably lower than hydraulic ones;

The electric ICV possesses an electromechanical device, attached to the sliding sleeve, which converts the electrical power to mechanical one to shift the valve to open, closed or any intermediate position. The choking of the valve can be directly measured by displacement sensors. Figure 21 show and electric valve in open and closed position with its main elements.
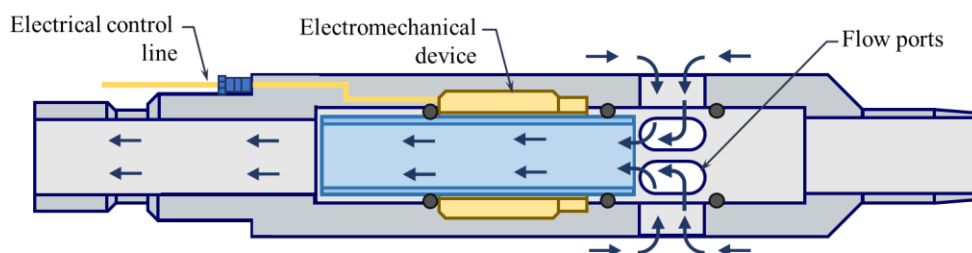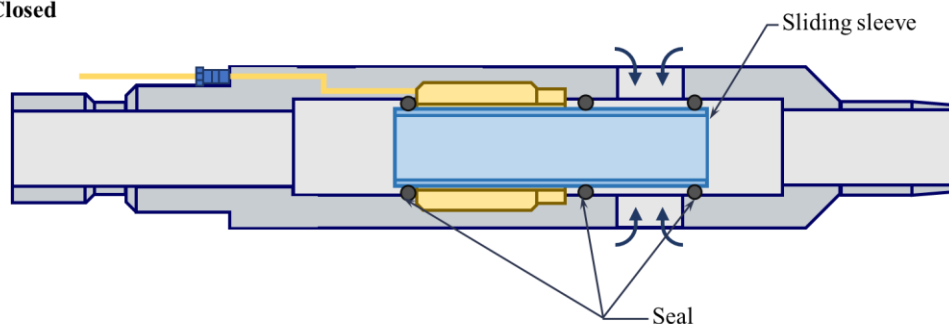
Figure 21: Electric ICV in open and closed positions with main components (Author)

In Figure 22, an all-electric IWC of a 3-zones well with one electric ICV per interval is shown. Operating the valves can be done through only one electric control line.
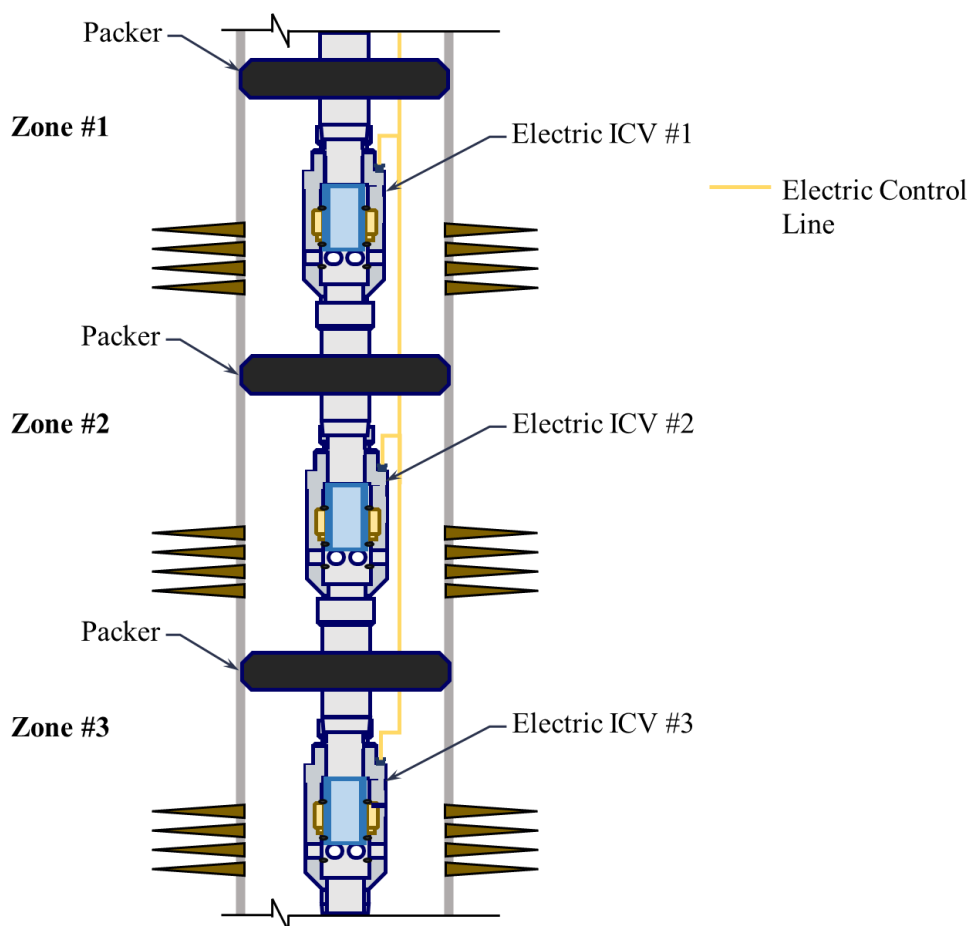
Figure 22: Well section schematic of a 3-zones electric IWC with one electric ICV per interval, packers separating each zone and a single electrical control line to control all the valves (Author)

2.2.4

Interval Control Valve versus Interval Control Device

Interval control devices (ICD) differ from ICVs conceptually as they are passive components in a completion. Once an ICD is installed, the flowing area from annulus to tubing through the tool cannot be changed. These devices, however, also have the function of controlling the fluid flow in a production zone by reducing its velocity. They are usually installed in sand control completions with high permeability to reduce coning tendencies. Figure 23 shows an example of an orifice type ICD showing schematically the flow path along its body.
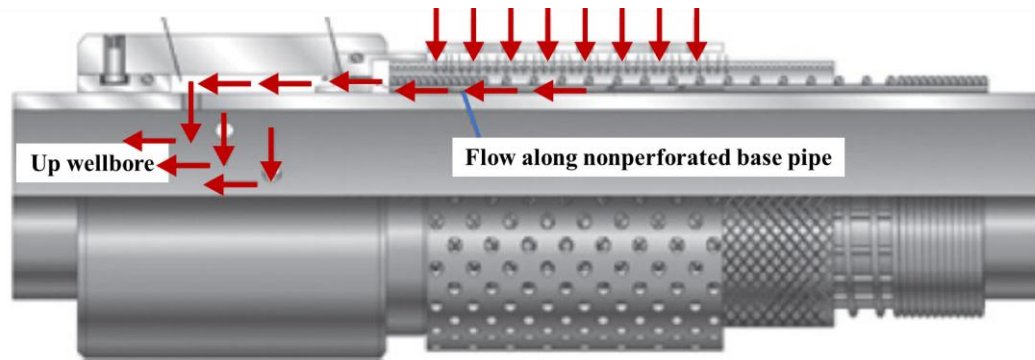
Figure 23: Example of an inflow control device (ICD): Orifice type (Adapted from [1]).

2.3
Development Methodology of New Completion Tools to be Installed in Intelligent Wells

The development of new completion tools, or any new product/technology, follows a methodology to assure that function, performance goals, technical requirements, and reduced risks are achieved so the unit can be released commercially. International standards, client technical specifications and specific custom tests can be adopted to ensure the functioning of the technology within the performance target, operational conditions, and expected lifetime.

The standard from the American Petroleum Institute, API 17Q [31], describes steps which guides the development of new subsea equipment and can also be extended to IWC components. Figure 24 shows nine steps, with their respective description, that a new development should follow to assure the progression of technology maturity through a technology readiness level (TRL) scale.

| STEP 1 | REQUIREMENTS AND GOALS DEFINITION | Requirements, goals and acceptance criteria of the technology for a qualification program are defined. |
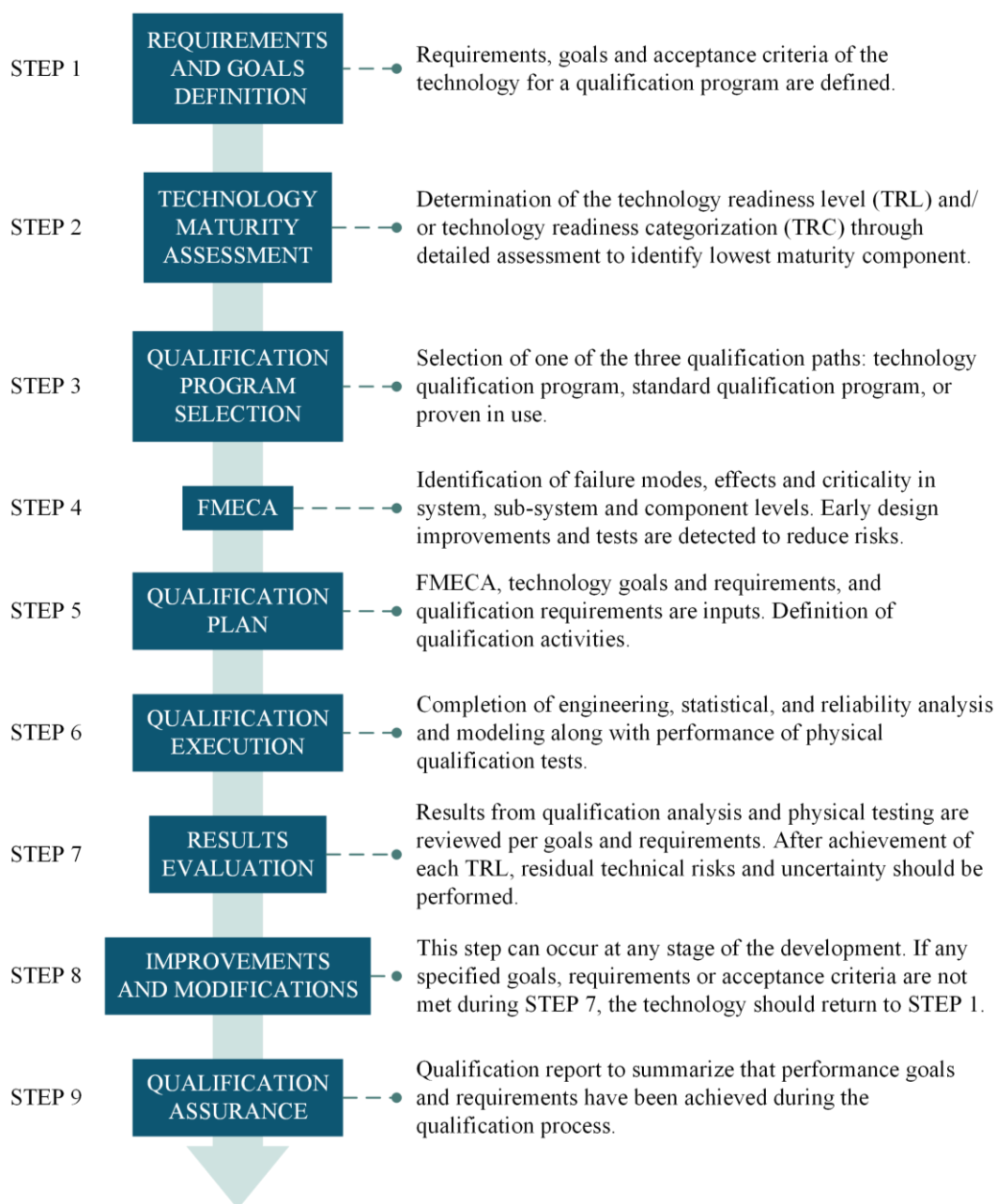
Figure 24: Technology development steps per API 17Q (Adapted from [31])

2.3.1

Technology Readiness Levels

Technology Readiness Level (TRL) is a scale for measuring the maturity of a technology. TRLs enable the standardized assessment of the maturity of a particular technology and the consistent comparison of the maturity between different types of technology in the context of a specific application, implementation, and operational environment [32]. The scale is widely used in Research and Development (R&D) projects and ranges from 1 to 9. Figure 25 shows

the TRL scale, with milestones' description slightly modified from NASA's reference ([32]), adopted by the oil companies' consortia that operates in the Brazilian Pre-Salt fields for development and installation of new well completion tools as observed by [33], [23], and [34].
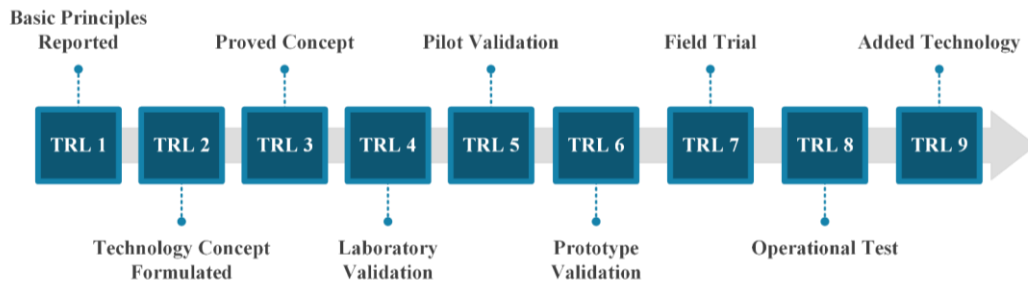
Figure 25: Modified technology readiness level scale adopted by Pre-Salt oil companies' consortia (Adapted from [31] and [32]).

Below are each TRL with a detailed description of the tasks necessary to achieve each level taken from [32] and [31]:

- TRL 1 (Basic Principles Reported) – Scientific and/or engineering basic principles reported; technology concept and application highlighted; fundamental objectives and requirements identified; sketches of basic form and functions; review of lessons learned from comparable technologies; key technical risks identified.

- TRL 2 (Technology Concept Formulated) – concept and application of technology formulated; functionality demonstration by analysis; preliminary fit assessment of physical interfaces; no experimental proof; update technical risks.

- TRL 3 (Proved Concept) – R&D is initiated; new features and concept design is concept-proven by physical model (system mock-up or dummy) tested in a laboratory; preliminary FMECA performed; engineering studies for function/performance/reliability specification; reliability drivers are identified; interfaces are all identified; update technical risks.

- TRL 4 (Laboratory Validation) – detailed FMECA performed; all finite element analysis (FEA), computational fluid dynamics (CFD), and hand calculations completed; system reliability analysis; component and sub-system level physical prototype function tested in laboratory; manufacturing,

assembly, transit, storage and/or installation risks addressed; estimation of reliability, residual technical risks, and uncertainty.

- TRL 5 (Pilot Validation) – review and update FMECA; performance data collection system defined; manufacturing and assembly process validated; full scale prototype built and tested per qualification program in simulated/relevant environment; reliability test of component/sub-system completed; update estimation of system reliability, residual technical risks, and uncertainty.

- TRL 6 (Prototype Validation) - review and update FMECA; full scale prototype is function/performance tested integrated with wider system outside of field environment; system reliability test and data collection completed.

- TRL 7 (Field Trial) – review and update FMECA; production unit built, installed, and commissioned into wider production system; detailed in-service inspection, monitoring, and sampling defined; verification of inspection, monitoring, and sampling functions; preparedness response defined; full interface and function qualification testing in actual operational environment; remaining technical risks to be managed by operations identified.

- TRL 8 (Operational Test) - production unit built and installed into operating system for two installations; in-service monitoring, sampling and inspection implementation; reliability and integrity performance data collected and analyzed; review and update FMECA with in-service data; perform root cause failure analysis (RCFA) for failed/underperforming components; reliability improvements for failed/underperforming components implemented; feedback performance to stakeholders.

- TRL 9 (Added Technology) – product implemented in final user/client portfolio.

2.3.2

API 19ICV – International Standard for Testing Interval Control Valves

As an industry effort to standardize the tests for interval control valves due to its importance to the IWC, the American Petroleum Institute (API) released in June

2023 the first edition of its ICV's specification, the API 19ICV [35]. Along with the client/oil operator's technical specification, this standard now can be considered as a "standard qualification program" to be used alone or as part of the "technology qualification program" per STEP 3 from API 17Q [31].

The API 19ICV stablishes three validation grades - V3, V2 and V1-, V3 being the least severe and V1 is the most severe. Table 2 below reproduces the standard's validation tests that are defined by the supplier or manufacturer, required, or not required for each grade.

Table 2: Validation tests requirement summary for each grade [35]

Validation Test	Validation Grade		
	V3	V2	V1
Static Pressure Integrity Test	Defined by supplier/manufacturer	Required	Required
Operating Cycle Test	Defined by supplier/manufacturer	Required	Required
Differential Unloading Test	Defined by supplier/manufacturer	Required	Required
Mechanical Integrity with Combined Loading Test	Not required	Not required	Required
Bend Test	Not required	Required	Required
Flow Characterization Test (Choking Valves Only)	Defined by supplier/manufacturer	CFD acceptable	Required
Production Erosion Test	Not required	Not required	Required
Flowing Differential Integrity Test	Not required	Not required	Required
Drift Test	Defined by supplier/manufacturer	Required	Required

Table 3 presents a description of testing requirements for the validation grades V2 and V1.

Table 3: Description of validation grades V2 and V1 testing requirements [35].

Validation Test	Validation Grade	
	V2	V1
Static Pressure Integrity Test	a) Apply pressure from internal to external the ICV at its rated pressure and at maximum and minimum rated temperatures. Hold for 15 minutes. b) Apply pressure from external to internal of the ICV at its rated pressure and at maximum and	a) Apply pressure from internal to external the ICV at its rated pressure and at maximum and minimum rated temperatures. Hold for 15 minutes. b) Apply pressure from external to internal of the ICV at its rated pressure and at maximum and

Validation Test	Validation Grade	
	V2	**V1**
	minimum rated temperatures. Hold for 15 minutes. c) Apply pressure to each pressure retaining chamber(s) of the ICV at respective rated pressure(s), as applicable to the design.	minimum rated temperatures. Hold for 15 minutes. c) Apply pressure to each pressure retaining chamber(s) of the ICV at respective rated pressure(s), as applicable to the design.
Operating Cycle Test	a) Perform a minimum of 60 operating cycles at maximum rated temperature. b) Perform a minimum of 60 operating cycles at minimum rated temperature. c) Perform a Static Pressure Integrity Test at the end of a) and b).	a) Perform a 3 operating cycles at ambient temperature. b) Perform a minimum of 80 operating cycles at maximum rated temperature. c) Perform a minimum of 80 operating cycles at minimum rated temperature. d) Perform 80 operating cycles (or enough to complete 240 cycles) at maximum, minimum, or both rated temperatures. e) Perform a Static Pressure Integrity Test at the end of a), b), c) and d).
Differential Unloading Test	a) Perform a minimum of 3 differential pressure unloads in each rated direction at maximum rated temperature. b) Perform a minimum of 3 differential pressure unloads in each rated direction at minimum rated temperature. c) Perform a Static Pressure Integrity Test at the end of a) and b).	a) Perform a minimum of 6 differential pressure unloads in each rated direction at maximum rated temperature. b) Perform a minimum of 6 differential pressure unloads in each rated direction at minimum rated temperature. c) Perform a Static Pressure Integrity Test at the end of a) and b).
Mechanical Integrity with Combined Loading Test	-	All tests are performed at maximum rated temperature. a) Apply the following from performance envelope: tensile load with internal pressure; tensile load with external pressure; compressive load with internal pressure; compressive load with external pressure. b) Perform a minimum of three operating cycles at the maximum rated tensile load without any pressure. c) Perform a minimum of three operating cycles at the maximum rated compressive load without any pressure. d) Perform a Static Pressure Integrity Test at the end of c).
Bend Test	Test shall be performed at ambient temperature. a) Perform a minimum of three operating cycles. b) Apply maximum RIH dog-leg rating for a minimum of five minutes in the close and fully open positions. c) Remove bending loads.	Test shall be performed at ambient temperature. a) Perform a minimum of three operating cycles. b) Apply maximum operating dog-leg rating and, while bending load is applied, perform a minimum of three operating cycles. c) If higher than the operating dog-leg rating, apply the maximum RIH dog-

Validation Test	Validation Grade	
	V2	**V1**
	d) Perform a Static Pressure Integrity Test (internal to external only) at the end of c) e) After bend test, perform a minimum of three operating cycles.	leg rating for a minimum of five minutes in the close and fully open positions. d) Remove bending loads. e) Perform a Static Pressure Integrity Test (internal to external only) at the end of c) f) After bend test, perform a minimum of three operating cycles.
Flow Characterization Test (Choking Valves Only)	a) Flow characterization and C_v versus choking position shall be determined by testing or CFD. a minimum of six choking positions, including smallest and largest choke positions. b) Numerical analysis (CFD) shall be validated against physical test on similar flow geometry from an existing ICV.	a) Flow with city water in a minimum of six choking positions, including smallest and largest choke positions, in all flowing direction per design. b) A minimum of three flow rates shall be measured for each choking position. Flow for a minimum of 10 minutes for each flow rate. c) Results shall be expressed as Valve Coefficient (C_v) for choke positions.
Production Erosion Test	-	a) The test shall be performed with sand slurry prepared as determined by the standard. b) Perform one operating cycle. c) Confirm flow coefficient before and after erosion test. d) The choke position shall provide a minimum 1% of flow area. e) Start the erosion test with maximum flowing differential pressure rating maintaining the 5-minute moving average flow rate within +/- 10% of initial flow rate. f) Test duration shall have a total of 24 hours that can be broken in intervals. g) After erosion test, perform a Static Pressure Integrity Test at the end of f).
Flowing Differential Integrity Test	-	a) Flow with city water in a choke position capable of reaching the maximum flowing differential pressure. b) Flow rate shall be either minimum of 12.4 ft/sec in the tubing size or maximum flow rate in the selected choking position. c) Flow at selected choking position at maximum rated flowing differential pressure for one hour constant within 5% of target flow rate using 5-minute moving average. d) Prior to starting the test and at the conclusion, perform one operating cycle and record actuation parameters.
Drift Test	a) Pass a drift bar, appropriate for tubing size, completely through the valve in both directions.	a) Pass a drift bar, appropriate for tubing size, completely through the valve in both directions.

It is also described by the standard three additional tests, listed in Table 4, which may be required by the end user.

Table 4: Additional tests requirements to be defined the need by manufacturer/supplier [35].

Additional Test	Requirements
System Integration Testing (SIT)	a) Demonstrate overall system functionality with all its components. b) Prove that the actuation of one ICV does not affect the functioning of other components and vice-versa.
Testing of the ICV with Absolute Pressure	a) Perform three operating cycles at ambient pressure and temperature. b) Perform three operating cycles at ambient temperature with 50% of maximum absolute pressure. c) Perform three operating cycles at ambient temperature with 100% of maximum absolute pressure. d) Perform the Static Pressure Integrity Test at ambient temperature.
Injection Erosion Test	a) The test shall be performed with sand slurry prepared as determined by the standard. b) Perform one operating cycle, confirm flow coefficient before and after erosion test. c) Start the erosion test with maximum flowing differential pressure rating maintaining the 5-minute moving average flow rate within +/- 10% of initial flow rate. d) The test duration shall have a total of 24 hours that can be broken in intervals. e) After erosion test perform external and internal static integrity pressure test to the rated pressure with the valve closed

3

Electric Interval Control Valve's Electromechanical Actuator Design

The Electric Interval Control Valve (ICV) was conceptually divided into sub-assemblies to make it possible to test and achieve the requirements for each of them. They are: the Electronics and Sensing Module, where the electronics for control and communication along with pressure and temperature, and linear displacement sensors are located; Actuation Module, which is comprised by the electromechanical actuator and its interfaces; and Flow Module, where the components exposed directly to the flow are located. Their location in the tool is shown in Figure 26.
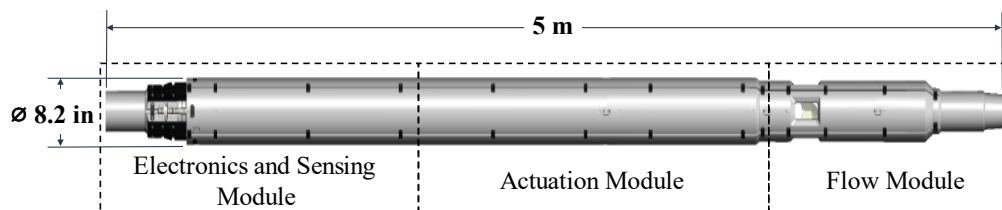
Figure 26: Electric ICV's modules for testing [24].

The tests listed below were performed successfully at sub-assembly level or full-scale prototype allowing the tool to progress to TRL4 in the technology maturity scale presented in Figure 25.

1.   Shock and vibration;
2.   Integrity tests;
    a.   Leakage
    b.   Axial loads
    c.   Cycling
3.   Differential pressure opening (unloading);
4.   Flow tests;
    a.   Flow characterization
    b.   Erosion

Figure 27a shows the Actuation Module's test fixture during the shock and vibration test combined with temperature. Figure 27b shows the test setup for the flow tests which the flow characterization and erosion tests were performed.
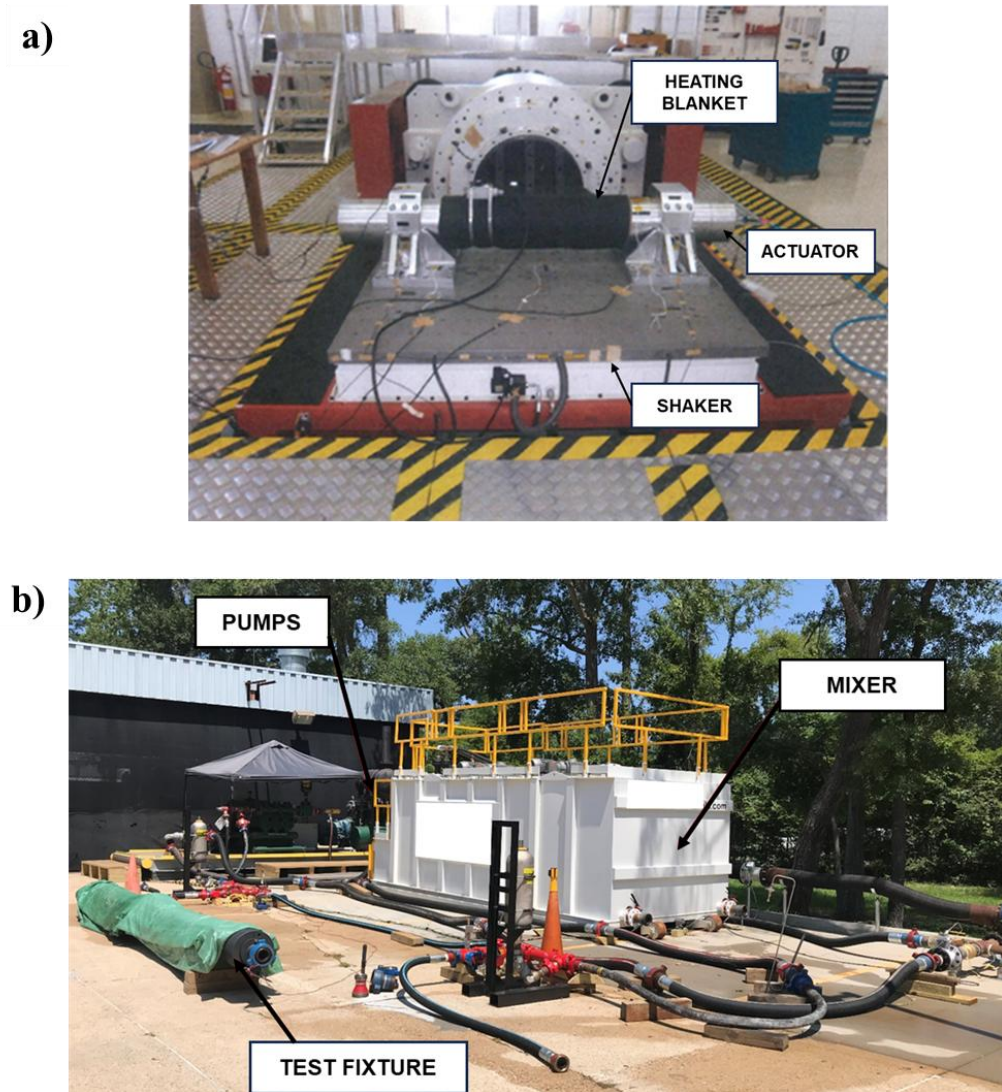
Figure 27: Tests performed with the actuator's module and full-scale prototype. a) Actuators module in the shock and vibration. b) Full-scale prototype erosion and flow characterization test setup [24]

The following subsections present the mathematical model, equations and calculations adopted for the electromechanical actuator's design. As illustrated by Figure 28, the workflow starts with the definition of the electrical power limitation from the power supply the Electric ICV is connected to. Then, the mathematical model, with all mechanical and electromechanical components identified, is defined to obtain the friction torques, related to the rotating elements, and friction forces, related to the friction of the sealing elements, through several equations. The outputs from the friction components are used as inputs to the mechanical actuator's

equation to give the minimum output actuation force for different scenarios considered.
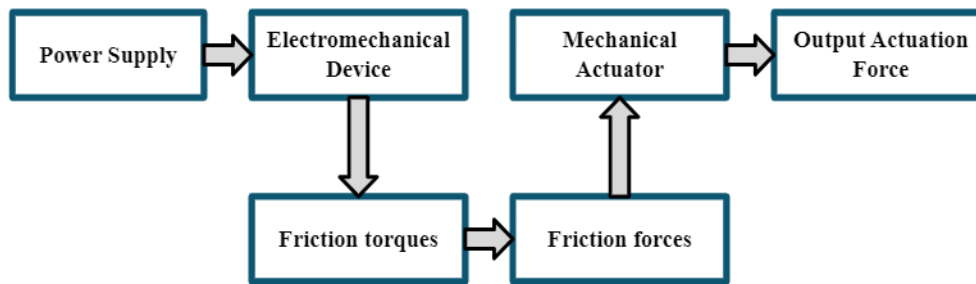
Figure 28: Electromechanical actuator's design workflow (Author)

3.1
Mathematical Model

The definition of the mathematical model starts with the identification of the components considered for the electromechanical actuator's analysis. The list below summarizes the function of each element shown in Figure 29:

- Electrical cable – provides the electrical power to the actuator through the control system from the Electronics and Sensing Module;

- Electromechanical device – Electric motor comprised by a fixed part and a rotating part to provide the required torque for the axial movement of the Sliding Sleeve;

- Axial bearing pre-load springs – spring used to provide the recommended pre-load to the axial bearing'

- Axial bearings - mechanical elements to support axial loads and reduce friction during the rotational motion of the electromechanical device and mechanical actuator;

- Sliding sleeve – mechanical component that is shifted to open or close the valve;

- Dynamic seals – set of sealing elements that seals the valve's inner chamber, where the electromechanical actuator's components are located, during the linear motion of the sliding sleeve;

- Radial bearings – mechanical elements to support radial loads, centralize and reduce friction between the rotation parts;

- Mechanical actuator – component responsible to convert the rotational motion from the electromechanical device into axial motion, converts torque into actuation force;

- Closing seal – set of sealing elements responsible for the complete closure of the valve to stop flow production or injection within the Electric ICV's installation section.
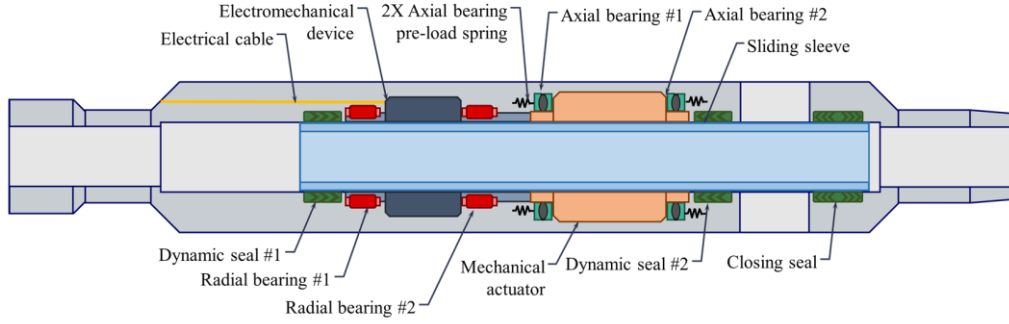
Figure 29: Electromechanical actuator's components considered for the analysis. (Author)

The electrical power is limited to $P_{e_{max}} = 200\ W$ and maximum voltage of $V_{max} = 400\ V$.

Most of the components mentioned previously have forces or torques associated during the actuation, as presented in Figure 30. $F_{fds_{1,2}}$ are the frictional forces from the dynamic seals #1 and #2, $T_{rb_{1.2}}$ are the frictional torques from the radial bearings #1 and #2, W_{rp} is the weight of the rotating parts, $F_{pl_{ab}}$ is the pre-load force acting on the axial bearings #1 and #2, T_{emd} is the torque the electromechanical device needs to provide for the valve actuation; $T_{ab_{1,2}}$ are the friction torques from the axial bearings #1 and #2, F_a is the actuation force the actuator provided during its movement, and F_{fcs} is the friction force from the closing seal.
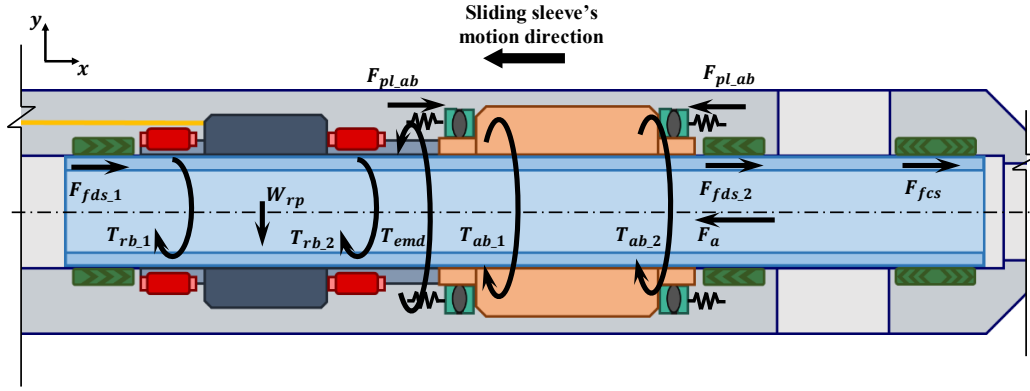
Figure 30: Torques and forces involved in the mathematical model of the electromechanical actuator (Author)

The electromechanical torque is the final value needed to define the power consumption of the system. It can be defined by the Eq. (3.1):

$$T_{emd} = k_t I \tag{3.1}$$

where k_t is the motor torque constant $[Nm/s]$ and I is the electric current $[A]$ applied to the electromechanical device. The electromechanical torque can also be written as a sum of the inertial torque ($J\alpha$), the viscous torque ($b_v\omega$) and the friction torques ($T_{friction}$) from the mechanical elements.

$$T_{emd} = k_t I = \underbrace{J\alpha}_{Inertial\ Torque} + \underbrace{b_v\omega}_{Viscous\ Torque} + \underbrace{T_{friction}}_{Mechanical\ Elements}$$

J is the second moment of mass $[kg \cdot m^2]$, α is the angular acceleration $[rad/s^2]$, b_v is the viscous coefficient of friction $[Nm/s]$, ω is the angular speed $[rpm]$ and $T_{friction}$ is the sum of frictional torques $[N]$.

For the analysis, the angular acceleration was considered zero as the electromechanical device's rotational movement was constant once set through the electronics control. This reduces T_{emd} to Eq. (3.2)

$$T_{emd} = \overbrace{J\alpha}^{zero\ as\ \alpha=0} + b_v\omega + T_{friction}$$

$$T_{emd} = b_v\omega + T_{friction} \tag{3.2}$$

3.2

Friction Torques Calculation

This section presents the equations and parameters used for the calculation through the model given by a bearing's manufacturer [36] for the calculation of the friction torques of both radial and axial bearings. Eq.(3.3) defines the frictional torques of bearings.

$$M_R = M_0 + M_1 \tag{3.3}$$

M_0 and M_1 are the sum of frictional torques, valid for radial bearings and axial bearings, as a function of the rotational speed and as function of load, respectively. Both M_0 and M_1 can be expanded with their respective subscripts as the assembly has two different sizes of radial bearings and one size of the axial bearing.

$$M_R = \underbrace{M_0}_{M_{0_{rb_1}}+M_{0_{rb_2}}+2M_{0_{ab}}} + \underbrace{M_1}_{M_{1_{rb_1}}+M_{1_{rb_2}}+2M_{1_{ab}}}$$

$M_{0_{rb_{1,2}}}$ are the frictional torques as function of speed while $M_{1_{rb_{1,2}}}$ are the frictional torques as a function of load for the radial bearings. $M_{0_{ab}}$ and $M_{1_{ab}}$ are the analogous for the axial bearing.

All the geometry and force factors for the radial and axial bearings used within the following equations are illustrated in Figure 31a and Figure 31b, respectively. Eq.(3.4) is applicable to both types of bearings for rotational speeds below 2000 rpm.

$$M_0 = f_0 160 d_M^3 10^{-7} \tag{3.4}$$

f_0 is the frictional torque bearing factor as a function of speed, d_M is the bearing's mean diameter. For the radial bearings, $f_{0_{rb}}$ is given by Eq. (3.5), which B_{rb} is the width and d_{rb} is the inner diameter of the bearing. The mean diameter, Eq. (3.6), is the same for all types of bearings.

$$f_{0_{rb}} = \frac{12 B_{rb}}{33 + d_{rb}} \tag{3.5}$$

$$d_M = \frac{d + D}{2} \tag{3.6}$$

The frictional torque as a function of load depends on the type of bearing being analyzed. Eq. (3.7) gives M_1 for the radial bearings and Eq.(3.8), for the axial bearing.

$$M_1 = f_{1_{rb}} F_r d_M \tag{3.7}$$

where $f_{1_{rb}} = 0{,}0005$ and F_r is the radial force acting on the bearing (here assumed as the weight of the rotating parts $F_r = W_{rp} g$).

$$M_1 = f_{1_{ab}} P_1 d_M \tag{3.8}$$

$f_{1_{ab}}$ is defined by Eq.(3.9) and P_1 is the decisive load given by Eq (3.10)

$$f_{1_{ab}} = 0{,}0012 \left(\frac{F_{pl_{ab}}}{C_0} \right)^{0.33} \tag{3.9}$$

$F_{pl_{ab}}$ is the axial load from the pre-load spring and C_0, Eq.(3.11), is the basic load given by [37].

$$P_1 = 3{,}3 F_{pl_{ab}} - 0{,}1 F_{r_{ab}} \tag{3.10}$$

$F_{r_{ab}}$ is the radial force acting on the axial bearing, which is zero for the system.

$$C_0 = f_{0_{ab}} Z D_W^2 \sin(\alpha_{ab}) \tag{3.11}$$

$f_{0_{ab}} = 1$ given by the manufacturer, Z is the number of balls within the axial bearing, D_W is the diameter of the balls and α_{ab} is the axial bearing load angle.
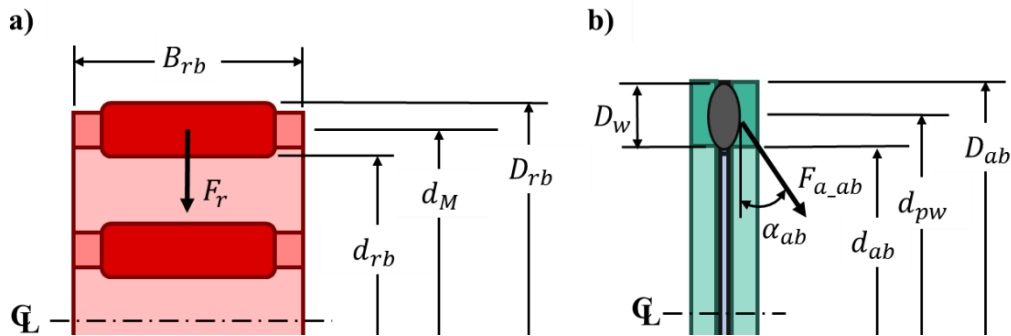
Figure 31:a) Radial bearings' geometry and force factors. b) Axial bearing' geometry and force factors. (Author)

The geometric factors used in the previous equations for the bearings' calculations are given in Table 5.

Table 5: Geometry factors for the radial and axial bearings.

Type	d [mm]	D [mm]	D_W [mm]	Z
Radial bearing #1	125	133	-	-
Radial bearing #2	130	137	-	-
Axial bearing	141	162	6,35	36

Finally, the calculated friction torque from the bearings (M_R) obtained is

$$M_R = \left(M_{0_{rb_1}} + M_{0_{rb_2}} + 2M_{0_{ab}} \right) + \left(M_{1_{rb_1}} + M_{1_{rb_2}} + 2M_{1_{ab}} \right)$$

$$\therefore M_R = 0,98 \, Nm$$

3.3
Friction Forces Calculation

The friction forces in the system are originated in both dynamic seals and closing seals, which are packs of V-Rings, during the movement of the sliding sleeve. Figure 32 shows an example of these type of seals.
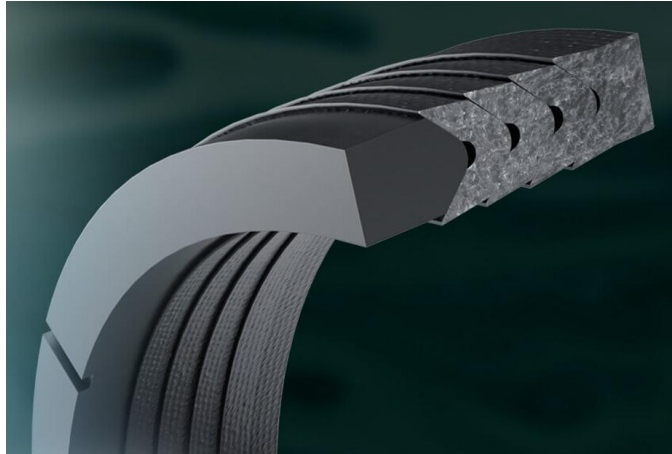
Figure 32: Example of Chevron/V-Ring pack type of dynamic seal [38]

Eq. (3.12) gives the friction from V-ring pack of seal, provided by a large seal manufacturer [39]. The equation has one term dependent on the differential pressure acting on the seal and another related to the seal squeeze during assembly inherent of its sealing function.

$$F_{friction} = \sum (\pi D\mu(\Delta p J_{seal} + S)) \tag{3.12}$$

D is the sealing diameter of the dynamic surface, μ is the coefficient of friction, Δp is the differential pressure on the seal V-ring, J_{seal} is the geometry factor for V-ring seals and S is the spring factor of the V-ring.

$$F_{friction} = \sum \left(\pi D\mu(\underbrace{\Delta p J_{seal}}_{due\ to\ pressure} + \underbrace{S}_{due\ to\ seal\ squeeze}) \right)$$

Eq. (3.13) shows the components of $F_{friction}$

$$F_{friction} = F_{fds_1} + F_{fds_2} + F_{fcs} \tag{3.13}$$

where $F_{fds_{1,2}}$ are the friction forces from the dynamic seals and F_{fcs} is the friction force from the closing seal. Both dynamic seals of the system are equal in geometry, material selection and number of V-rings. Eqs. (3.14) and (3.15) expand Eq. (3.12) with the subscripts for each V-Ring material, D becomes D_{sl}, the sliding sleeve's outer diameter ($D_{sl} = 4,5\ in = 114,3\ mm$), and the addition of the term N for the number of V-Rings multiplying the terms.

$$F_{fds_1} = F_{fds_2} = N_{MSE}\left(\pi D_{sl}\mu_{PTFE}(\Delta p J_{MSE} + S_{MSE})\right)$$
$$+ N_{PTFE}\left(\pi D_{sl}\mu_{PTFE}(\Delta p J_{MSE} + S_{PTFE})\right) \tag{3.14}$$

$$F_{fcs} = N_{PEEK}\left(\pi D_{sl}\mu_{PEEK}(\Delta p J_{PEEK} + S_{PEEK})\right) \tag{3.15}$$

All geometry factors, number of V-rings and respective materials are shown in Figure 33a and Figure 33b. Figure 33c shows the J_{seal} factor.
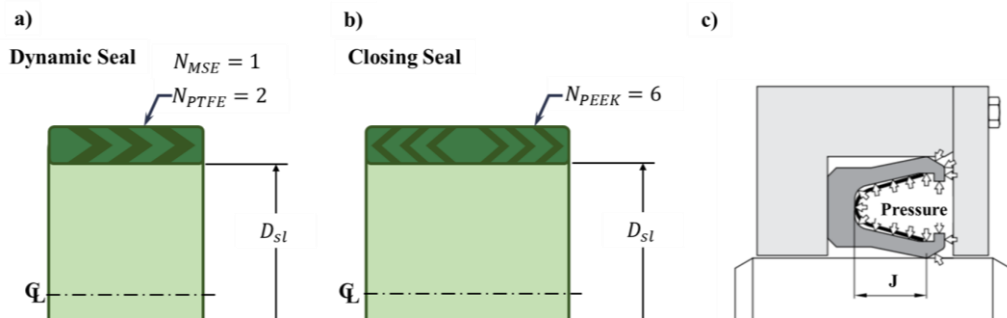
Figure 33: a) Dynamic seal geometry factor and number of MSE and PTFE V-Rings with different specifications. b) Closing seal geometry factor and number of PEEK V-Rings. c) Chevron/V-ring seal geometry factor "J" and working principle (Author and adapted from [39])

Table 6 shows the values for the geometry and number of V-rings used in Eqs. (3.14) and (3.15).

Table 6: Values of the factors used for calculation of the friction forces for different seal materials

	MSE	PEEK	PTFE
$N_{\square}$	1	6	2
J_{seal} [mm]	4,37	2,57	1,64
$S_{\square}$ [N/mm]	10	3,18	0,50
$\mu_{\square}$	0,10	0,35	0,10

3.3.1

Test Scenarios for the Analysis

To identify the scenarios which, the friction forces from the seals change depending on the differential pressure (Δp). For all scenarios, the valve is shown in the closed position to analyze the worst case of friction forces during the sliding sleeve's movement.

The differential pressure acting on the valve body during the cycling tests, shown in Figure 34, is 10.000 psi as the inner chamber, where the electromechanical components are located, has atmospheric pressure ($p_i = 0\ psi$).
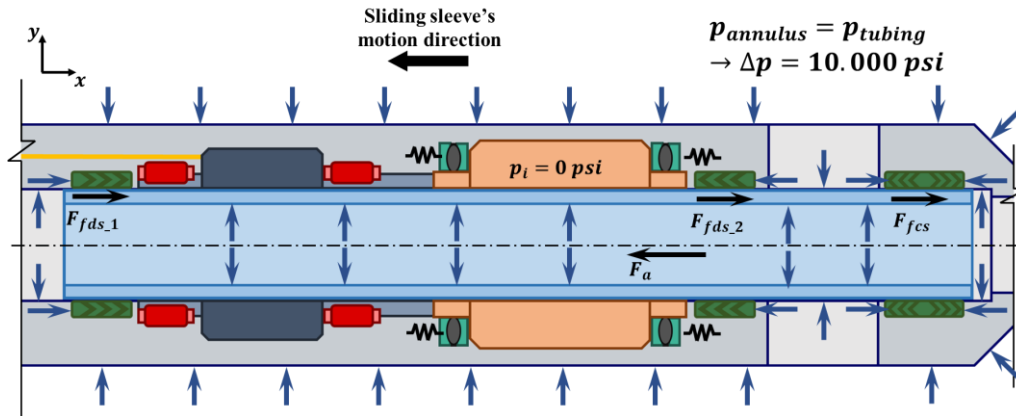
Figure 34: Pressure and friction forces acting on seals during cycling test. (Author)

The other relevant scenario is during the Differential Pressure Opening test which the valve is open with 1.500 psi of differential pressure either from the tubing to annulus side (Δp_{tubing}) or vice versa ($\Delta p_{annulus}$). Figure 35a shows the first case and Figure 35b shows the second one.
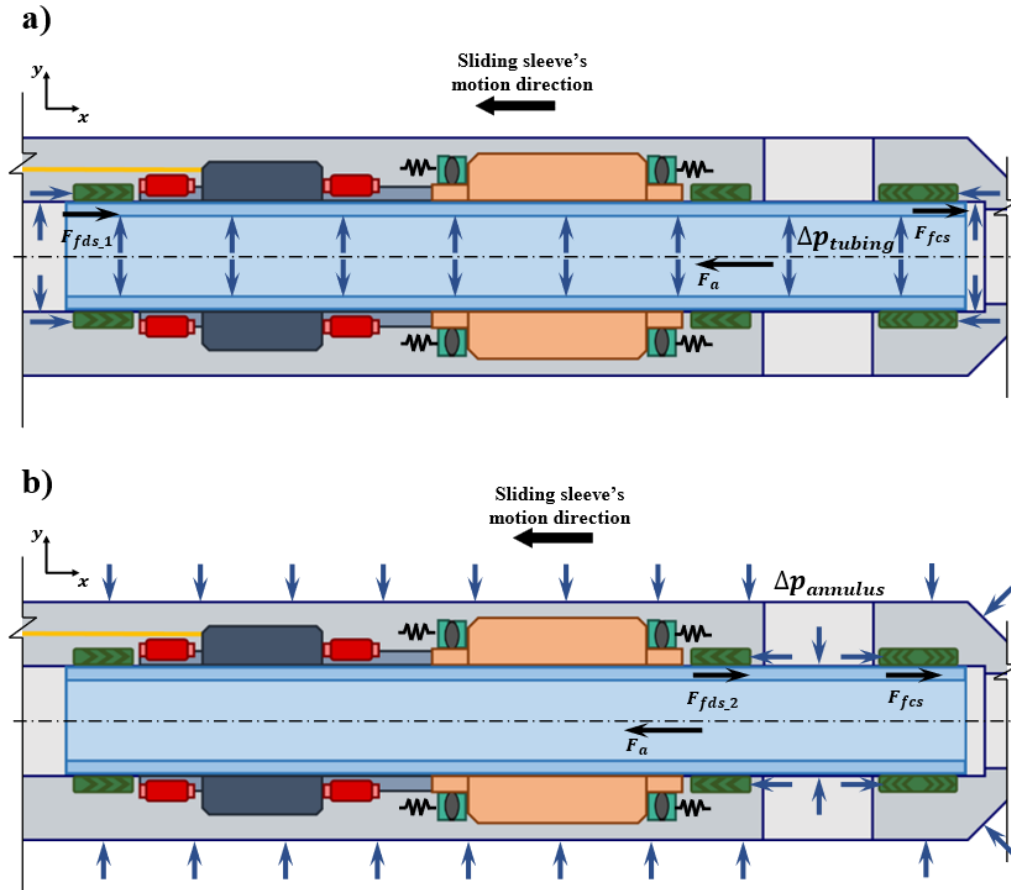
Figure 35: Friction forces acting on seals during differential pressure opening test. a) Differential pressure from tubing to annulus. b) Differential pressure opening from annulus to tubing. (Author)

In Table 7, the differential pressures, considered for the design and further comparison with experimental data, acting on the dynamic seals (Δp_{ds}) or closing seals (Δp_{cs}) are summarized.

Table 7: Differential pressures acting on the dynamic seals and closing seal.

Δp_{ds} [psi]	Δp_{cs} [psi]
0	0
1500	1500
10000	0

3.4

Actuation Force and Torque Calculation

The mechanical actuator, which is a ball screw, is responsible for the conversion of torque into actuation force. Figure 36 shows the geometry factors of the ball screw and its main components.
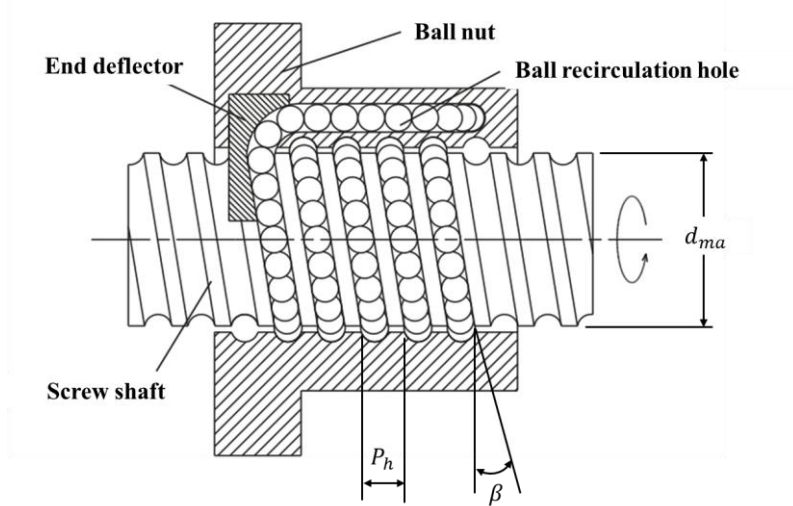
Figure 36:Mechanical actuator's geometry factors and main components (Adapted from [40])

The lead angle (β), is the geometry factor directly related to the mechanical efficiency. It is dependent of the ball screw's pitch (P_h) and diameter (d_{ma}) as shown in Eq.(3.16)

$$\beta = \tan^{-1}\left(\frac{P_h}{\pi d_{ma}}\right) \qquad (3.16)$$

which gives

$$\boldsymbol{\beta = 0,54°}$$

From β, the mechanical actuator's efficiency can be obtained from the manufacturer's efficiency plot for three different coefficients of friction [40]

$$\mu = \begin{bmatrix} 0,003 \\ 0,005 \\ 0,1 \end{bmatrix}$$

which were considered to obtain three different mechanical actuator's efficiencies (η_{ma}) used throughout the study. The efficiencies obtained are shown in the plot, Figure 37.
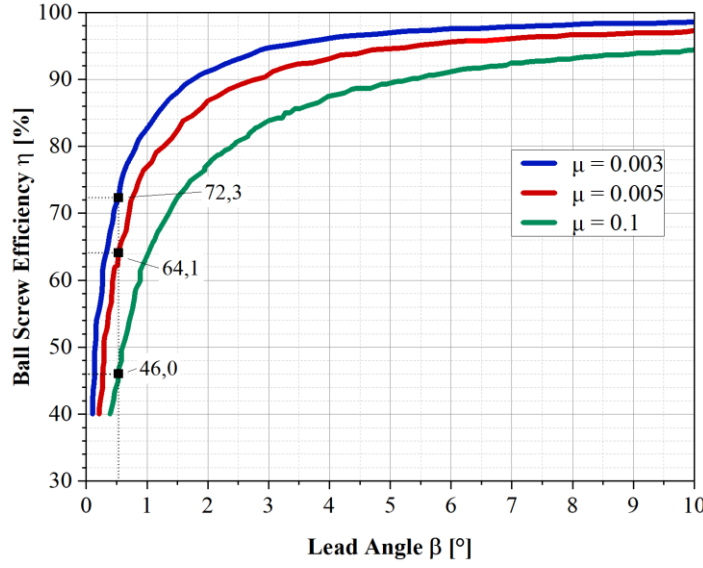
Figure 37:Mechanical actuator's efficiency plot as function of the lead angle and coefficient of friction. Three efficiencies for lead angle ($\boldsymbol{\beta = 0,54°}$) of the mechanical actuator analyzed are highlighted for each curve (Digitized and adapted from [40])

The mechanical actuator's efficiencies

$$\eta_{ma} = \begin{bmatrix} 46,0 \\ 64,1 \\ 72,3 \end{bmatrix} \%$$

are used as input in the equation that gives the actuation torque (T_a), Eq. (3.17),

$$T_a = \frac{F_a P_h}{2\pi\eta_{ma}} \tag{3.17}$$

where F_a is the actuation force that is the same as the friction force ($F_{friction}$) originated by the dynamic and closing seals.

$$F_a = F_{friction}$$

3.5
Graphical Analysis of Calculated Results

The results from the analyses throughout the previous sections are the used as inputs in the Eq. (3.18), which is the Eq. (3.2) rewritten showing the calculated terms of $T_{friction}$.for the electromechanical torque (T_{emd}).

$$T_{emd} = b_v\omega + \underbrace{M_R + T_a}_{T_{friction}} \tag{3.18}$$

The viscous coefficient of friction (b_v) is an experimental data that was assumed to be

$$b_v = 0{,}2 \; Nm \cdot s$$

for the design calculations. The different values of T_{emd} obtained for the combinations of the mechanical actuator's efficiencies and differential pressures are implemented in Eq. (3.19) along with different rotational speeds (ω) to obtain the mechanical power (P_m).

$$P_m = \omega T_{emd} \tag{3.19}$$

Finally, the mechanical power is divided by the electromechanical efficiency (η_{em}) assumed as 70% to give the electrical power (P_e) shown in Eq. (3.20).

$$P_e = \frac{P_m}{\eta_{em}} \tag{3.20}$$

The electrical power results from the calculation methodology herein presented for the design of the electromechanical actuator, for the three different mechanical efficiencies and differential pressures that occur during the tests, are presented in Figure 38a for $\eta_{ma} = 46\%$, Figure 38b for $\eta_{ma} = 64{,}1\%$ and Figure 38c for $\eta_{ma} = 72{,}3\%$.
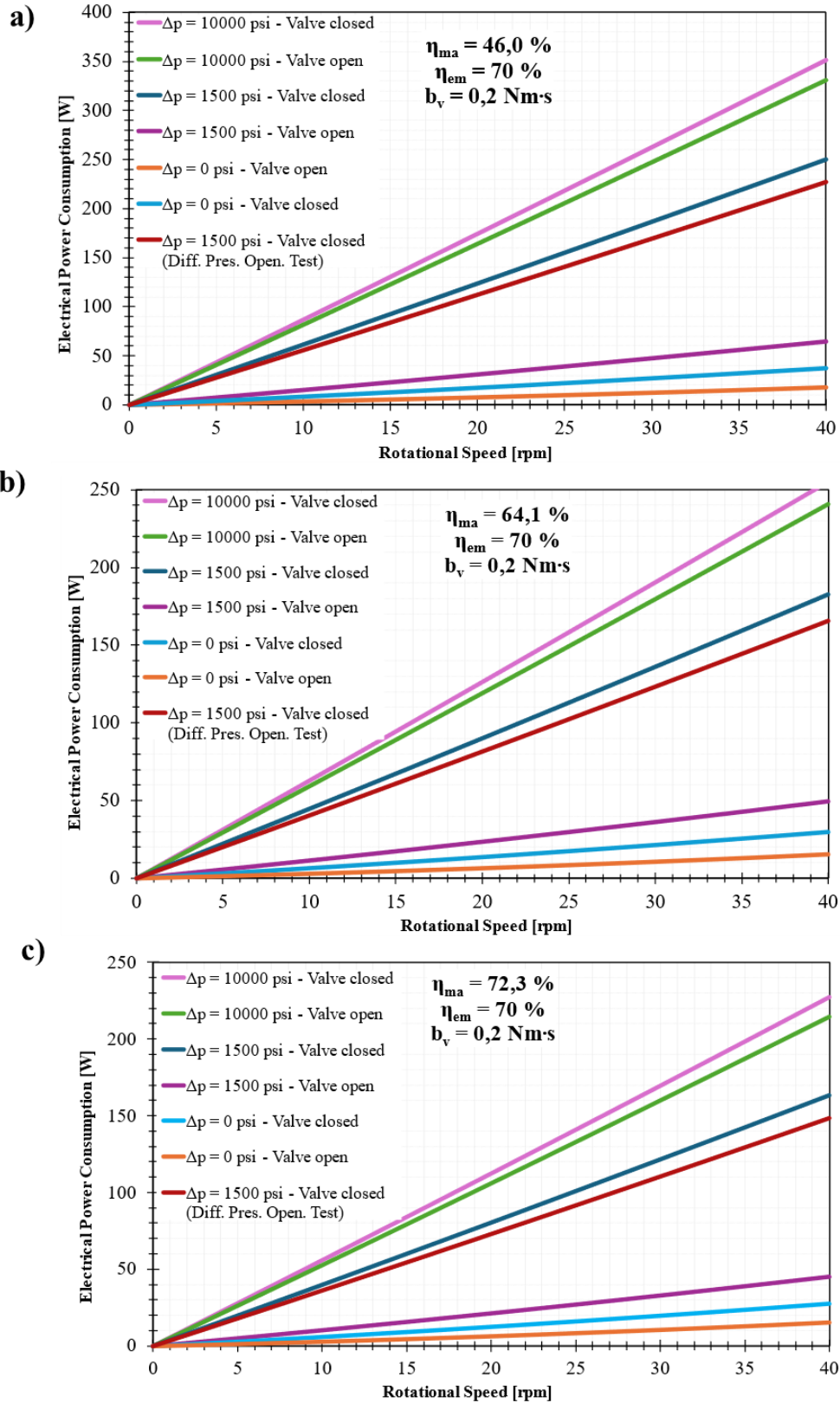
Figure 38: Graphical analysis of the power consumption as a function of the rotational speed for different operational conditions and different mechanical actuator`s efficiency. a) 46,0%. b) 64,1%. c) 72,3%. (Author)

4

Prototype Tests in the Laboratory Environment

The full-scale prototype of the Electric Interval Control Valve (ICV) was tested in a laboratory environment. The experimental data used for further comparison with the calculated results were originated from the following tests:

- Functional test at room temperature and no differential pressure
- Cycling test at maximum temperature and 10.000 psi
- Differential pressure opening test

They were all performed inside the same pressure chamber in a test cell as shown in Figure 39: Full-scale Electric Inflow Control Valve prototype for the Cycling and Differential Pressure Opening Tests (adapted from [24])Figure 39.
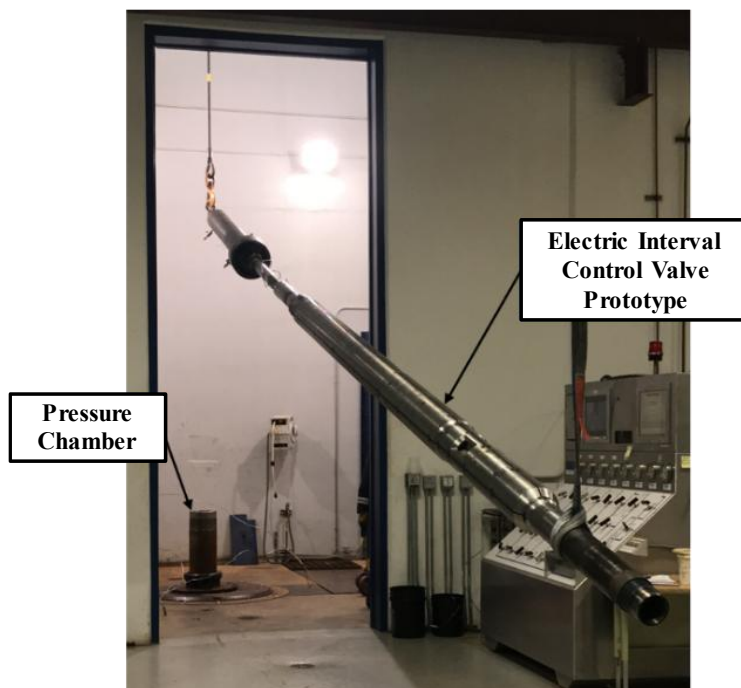
Figure 39: Full-scale Electric Inflow Control Valve prototype for the Cycling and Differential Pressure Opening Tests (Adapted from [24])

4.1

Experimental Data

The data presented in the following subsections were obtained from the tests performed with the full-scale prototype. They are used to compare and validate the electromechanical modelling of the Electric ICV's actuator. The electric power

consumption (P_e) and torque (T) are calculated from Eqs. (4.1) and (4.2), respectively. The next subsections present the electrical power consumption, torque, speed, and linear position of the sliding sleeve through time.

$$P_e = V_{in}I_{in} \tag{4.1}$$

$$T = k_t I_{in} \tag{4.2}$$

The input voltage (V_{in}), input electrical current (I_{in}), rotational speed given in rpm, and the linear displacement position of the valve are measurements provided by the control electronics and sensors inside the Electric ICV. The motor torque constant (k_t) in Eq. (4.2) is given by the motor characteristics.

4.1.1
Functional Test at Room Temperature and no Differential Pressure

Before starting the sequence of cycling and differential pressure opening tests at 10°C and 150 °C with differential pressures applied, a functional test to check the actuation and sensors proper work was performed. The test was performed at room temperature, measured as 27,4 °C, and no differential pressure was applied. In Figure 40 the data obtained from the test are plotted for one cycle of full opening and closing the valve. For all the plots, a moving average of fifteen points are included for each parameter. Figure 40a shows the speed, in rpm, and electrical power versus time, Figure 40b shows the speed and torque versus time, Figure 40c shows the electrical power consumption and torque versus time, and Figure 40d shows the linear position of the valve and electrical power consumption versus time.

Figure 40: Experimental data from the functional test at room temperature and no differential pressure plotted with moving average of 15 points for every parameter. a) Speed, in rpm, and electrical power versus time. b) Speed and torque versus time. c) Electrical power consumption and torque versus time. d) Linear position of the valve and electrical power consumption versus time. (Author and [41])

4.1.2

Cycling Test at Maximum Temperature and 10.000 psi

Proceeding with the test plan, the cycling test, in which the valve was shifted from full closed to the fully open position then to closed position 240 times, was performed. Figure 41 shows the schematic of the pressure acting across the body of the Electric ICV during the test.
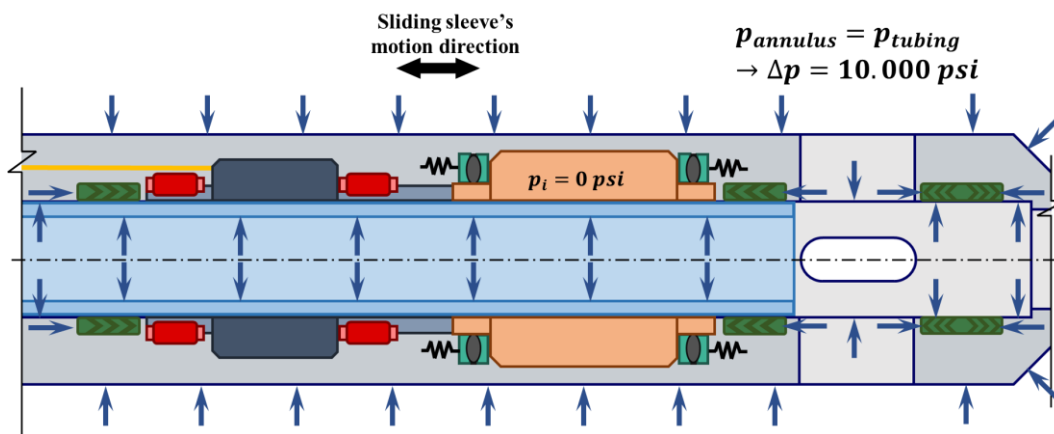
Figure 41: Schematics of the pressures acting across the Electric ICV's body during the cycling tests. (Author)

Figure 42 presents the data obtained from the cycling test at 150°C where near 40 cycles are performed during the timeframe presented. All the plots have the

moving average of fifteen points included for each parameter. Figure 42a shows the speed, in rpm, and electrical power versus time, Figure 42b shows the speed and torque versus time, Figure 42c shows the electrical power consumption and torque versus time, and Figure 42d shows the linear position of the valve and electrical power consumption versus time.
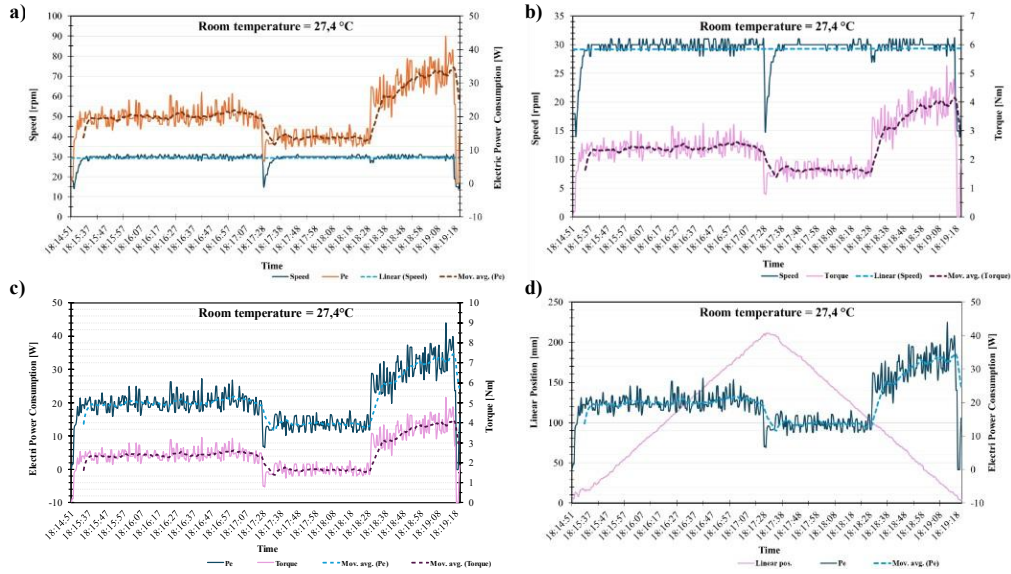

Figure 42: Experimental data from the cycling test at 150 °C and 10.000 psi of pressure across the valve plotted with moving average of 15 points for every parameter. a) Speed, in rpm, and electrical power versus time. b) Speed and torque versus time. c) Electrical power consumption and torque versus time. d) Linear position of the valve and electrical power consumption versus time. (Author and [41])

4.1.3

Differential Pressure Opening Test

The differential pressure opening test aims to evaluate the valve capability to open while a differential pressure is applied either in the injection mode (tubing to annulus), Figure 43a, or in the production mode (annulus to tubing), Figure 43b.
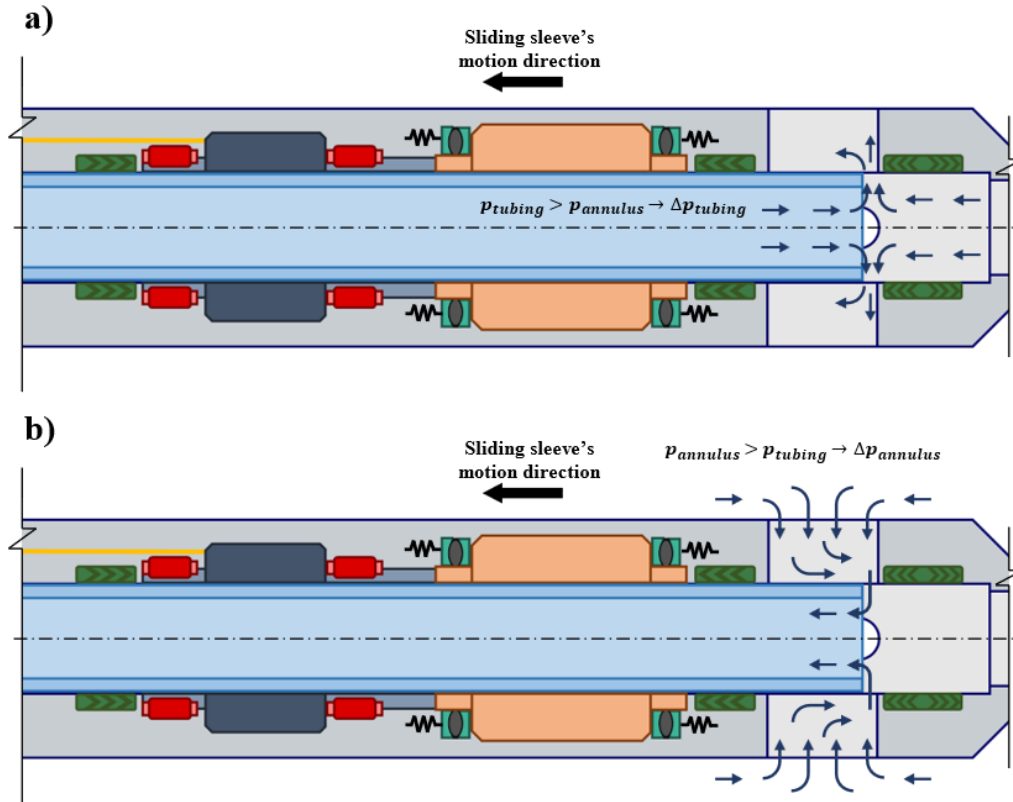
Figure 43: Schematics of the differential pressure opening test showing fluid unloading. a) Tubing to annulus differential pressure opening. b) Annulus to tubing differential pressure opening. (Author)

4.1.3.1

Differential Pressure of 1.500 psi from Tubing to Annulus at Low Temperature

Figure 44 shows the data obtained from the differential pressure opening test, with 1.500 psi of differential pressure from tubing to annulus, at 10°C during one cycle of opening and closing the valve during the timeframe presented. All the plots have the moving average of fifteen points included for each parameter. Figure 44a shows the speed, in rpm, and electrical power versus time, Figure 44b shows the speed and torque versus time, Figure 44c shows the electrical power consumption and torque versus time, and Figure 44d shows the linear position of the valve and electrical power consumption versus time.
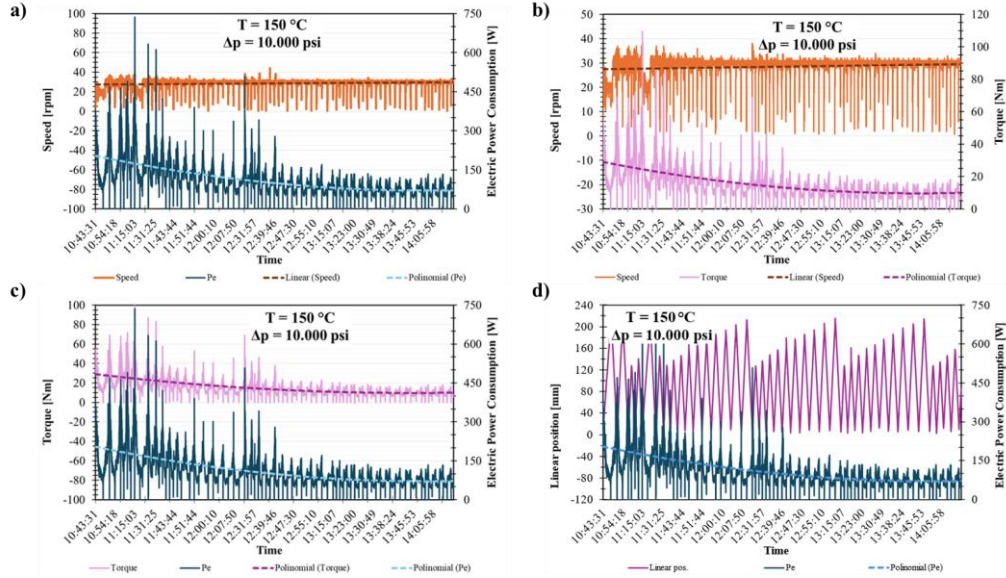
76

Figure 44: Experimental data from the differential pressure opening test at 10 °C and 1.500 psi of differential pressure from the tubing to the annulus side of the valve plotted with moving average of 15 points for every parameter. a) Speed, in rpm, and electrical power versus time. b) Speed and torque versus time. c) Electrical power consumption and torque versus time. d) Linear position of the valve and electrical power consumption versus time. (Author and [41])

4.1.3.2

Differential Pressure of 1.500 psi from Annulus to Tubing at Low Temperature

Figure 45 shows the data obtained from the differential pressure opening test, with 1.500 psi of differential pressure from annulus to tubing, at 10°C during one cycle of opening and closing the valve during the timeframe presented. All the plots have the moving average of fifteen points included for each parameter. Figure 45a shows the speed, in rpm, and electrical power versus time, Figure 45b shows the speed and torque versus time, Figure 45c shows the electrical power consumption and torque versus time, and Figure 45d shows the linear position of the valve and electrical power consumption versus time.

Figure 45: Experimental data from the differential pressure opening test at 10 °C and 1.500 psi of differential pressure from the annulus to the tubing side of the valve plotted with moving average of 15 points for every parameter. a) Speed, in rpm, and electrical power versus time. b) Speed and torque versus time. c) Electrical power consumption and torque versus time. d) Linear position of the valve and electrical power consumption versus time. (Author and [41])

4.1.3.3

Differential Pressure of 1.500 psi from Tubing to Annulus at High Temperature

Figure 46 presents the data obtained from the differential pressure opening test, with 1.500 psi of differential pressure from tubing to annulus, at 150°C during one cycle of opening and closing the valve during the timeframe presented. All the plots have the moving average of fifteen points included for each parameter. Figure 46a shows the speed, in rpm, and electrical power versus time, Figure 46b shows the speed and torque versus time, Figure 46c shows the electrical power consumption and torque versus time, and Figure 46d shows the linear position of the valve and electrical power consumption versus time.
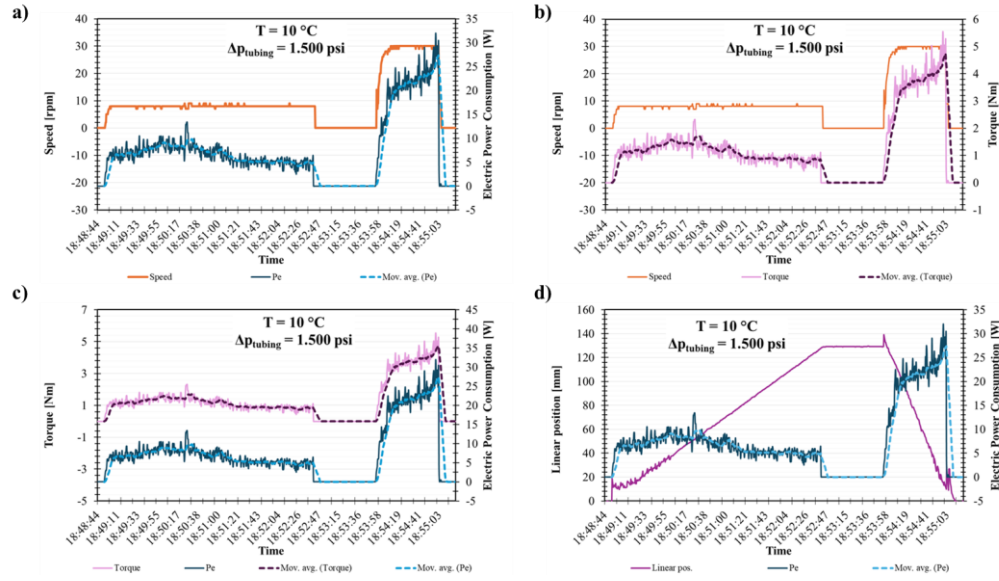
Figure 46: Experimental data from the differential pressure opening test at 150 °C and 1.500 psi of differential pressure from the tubing to the annulus side of the valve plotted with moving average of 15 points for every parameter. a) Speed, in rpm, and electrical power versus time. b) Speed and torque versus time. c) Electrical power consumption and torque versus time. d) Linear position of the valve and electrical power consumption versus time. (Author and [41])

4.1.3.4

Differential Pressure of 1.500 psi from Annulus to Tubing at High Temperature

Figure 47 presents the data obtained from the differential pressure opening test, with 1.500 psi of differential pressure from annulus to annulus, at 150°C during one cycle of opening and closing the valve during the timeframe presented. All the plots have the moving average of fifteen points included for each parameter. Figure 47a shows the speed, in rpm, and electrical power versus time, Figure 47b shows the speed and torque versus time, Figure 47c shows the electrical power consumption and torque versus time, and Figure 47d shows the linear position of the valve and electrical power consumption versus time.
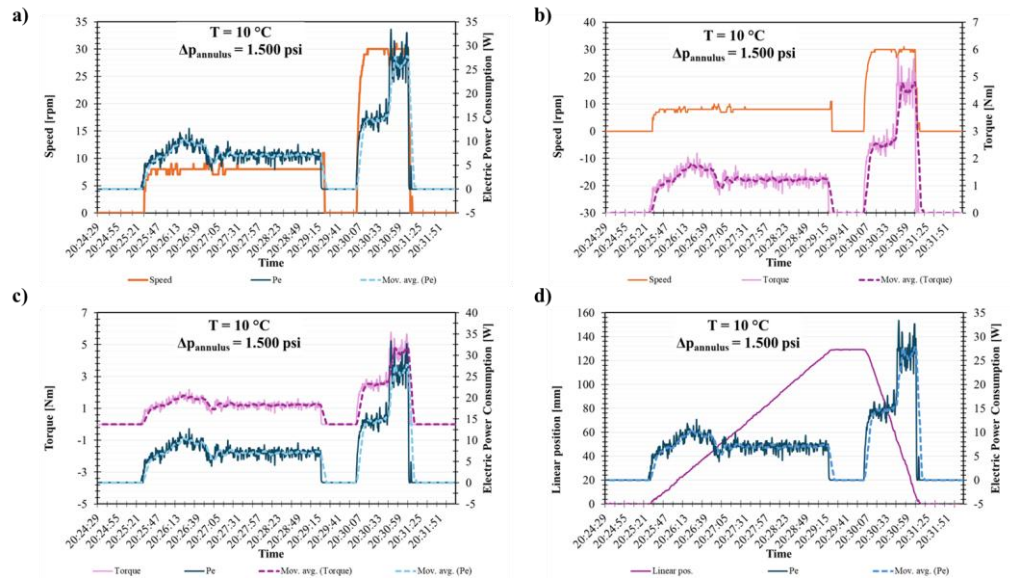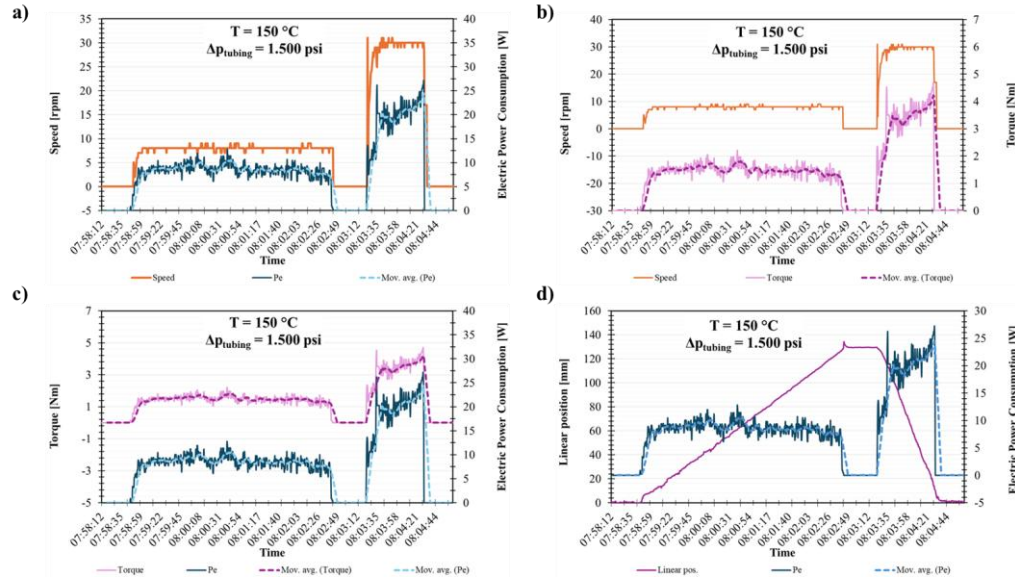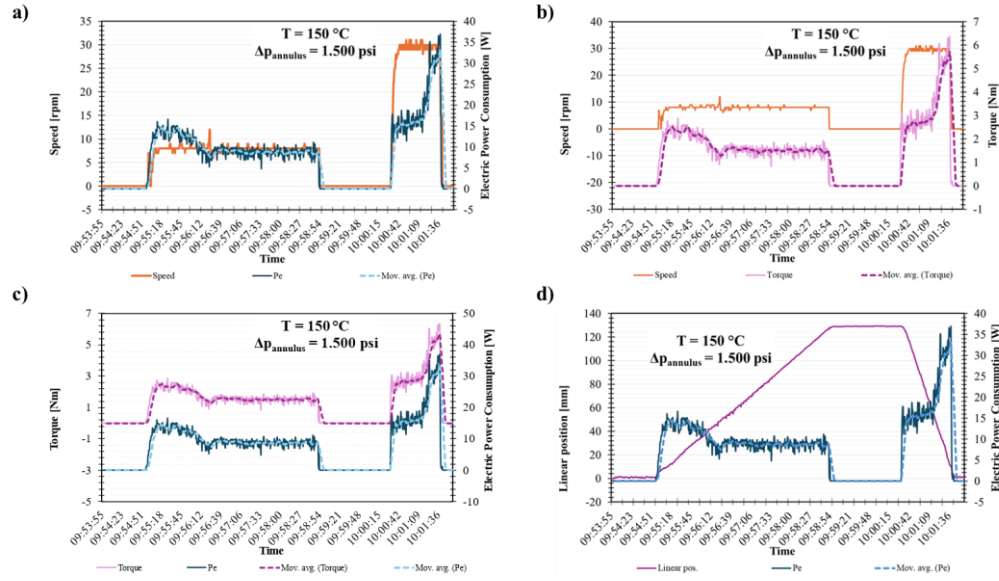
Figure 47: Experimental data from the differential pressure opening test at 150 °C and 1.500 psi of differential pressure from the annulus to the tubing side of the valve plotted with moving average of 15 points for every parameter. a) Speed, in rpm, and electrical power versus time. b) Speed and torque versus time. c) Electrical power consumption and torque versus time. d) Linear position of the valve and electrical power consumption versus time. (Author and [41])

4.2

Comparison Between Calculation Results and Experimental Data

This section presents the comparison of the results from the electromechanical design calculations and the experimental data from the full-scale prototype tests. The evaluations are performed for the functional test at room temperature, cycling test at high temperature and differential pressure opening test at low and high temperature during the opening and closing movement of the sliding sleeve. This aims to show the differences and similarities between the theoretical, considering the three different mechanical actuator's efficiencies (η_{ma}), and the actual results.

$$\eta_{ma} = \begin{bmatrix} 46,0 \\ 64,1 \\ 72,3 \end{bmatrix} \%$$

The comparison plots of the following subsections consider the location of the sliding sleeve during the opening and closing movement. As shown in Figure 48a, through distance "A" the actuation system will experience the friction from both dynamic seals ($F_{fds_{1,2}}$) and the valve closing seal (F_{fcs}). Figure 48b shows that

after leaving the closing seal section, the system will have the friction forces from the dynamic seals ($F_{fds_{1,2}}$) only.
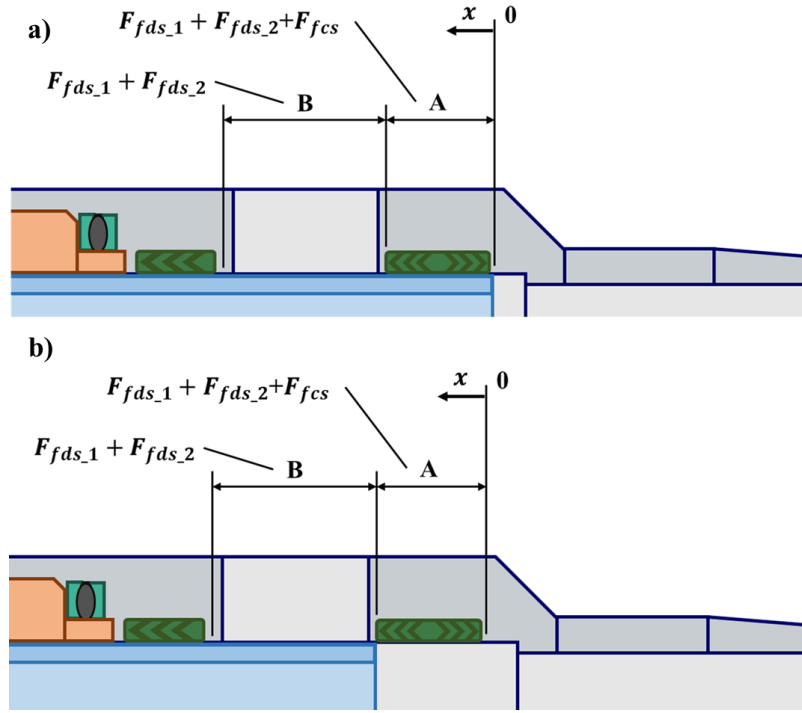
Figure 48: Friction forces the electromechanical actuator needs to overcome through different valve stages. a) Dynamic seals and closing seal friction through distance "A". b) Only dynamic seals friction through distance "B". (Author)

The precision of the mathematical model used through the electromechanical actuator's design is then assessed by means of the electrical power consumption and torque versus the linear position of the valve during the tests.

4.2.1
Functional Test at Room Temperature

Figure 49 presents the comparison plots for the electrical power consumption (Figure 49a), which from 0 to 80 mm, along the closing seal section, the calculated values were relatively precise for $\eta_{ma} = 72,3\%$, and torque (Figure 49b) that had a good precision through 80 to 180 mm, past the closing seal section, for $\eta_{ma} = 64,1\%$ and $\eta_{ma} = 72,3\%$, during the valve opening movement. A similar comparison for the closing movement is presented in Figure 50, where Figure 50a shows the electrical power consumption, with relative good precision for $\eta_{ma} = 46,0\%$ from 0 to 80 mm and for all three η_{ma} from 80 mm to 180 mm . AS for the torque (Figure 50b), $\eta_{ma} = 64,1\%$ and $\eta_{ma} = 72,3\%$ presented the closest results.

For both plots, it is important to note that the behavior of the experimental curve is highly aligned with the results from the calculations.
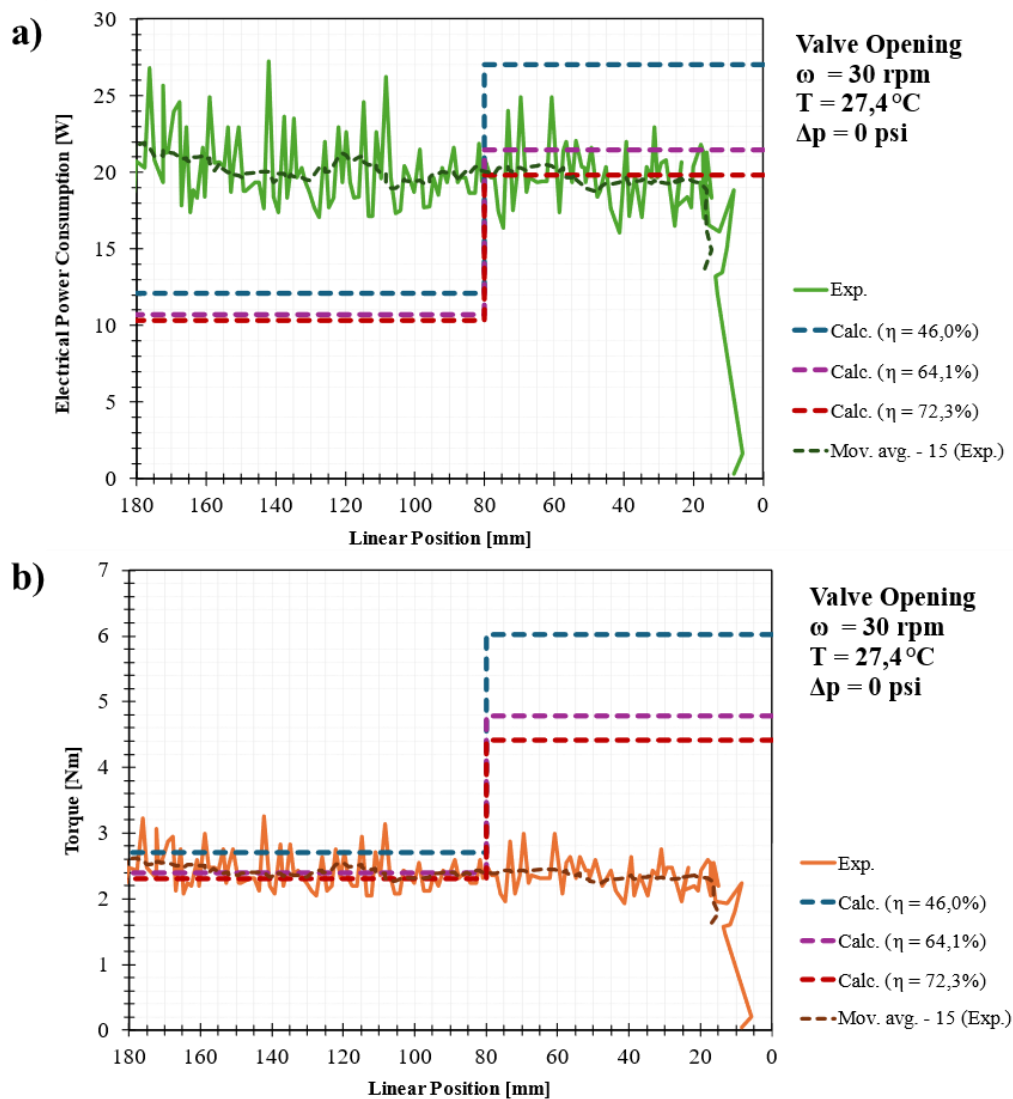
Figure 49: Comparison between calculated results and experimental data for the functional test at room temperature and no differential pressure for the opening movement of the sliding sleeve. a) Electrical power consumption versus linear position. b) Torque versus linear position (Author)

Figure 50: Comparison between calculated results and experimental data for the functional test at room temperature and no differential pressure for the closing movement of the sliding sleeve. a) Electrical power consumption versus linear position. b) Torque versus linear position (Author)

4.2.2

Cycling Test at High Temperature

Figure 51 presents the comparison plots for the electrical power consumption (Figure 51a) and torque (Figure 51b) for the cycling test at 150 °C .with 10.000 psi of differential pressure with the valve opening. The empirical results had lower values than originally predicted showing the model to be very conservative for this test condition. Figure 52, for the closing movement, also had conservative results for both electric power consumption (Figure 52a). and torque (Figure 52b).
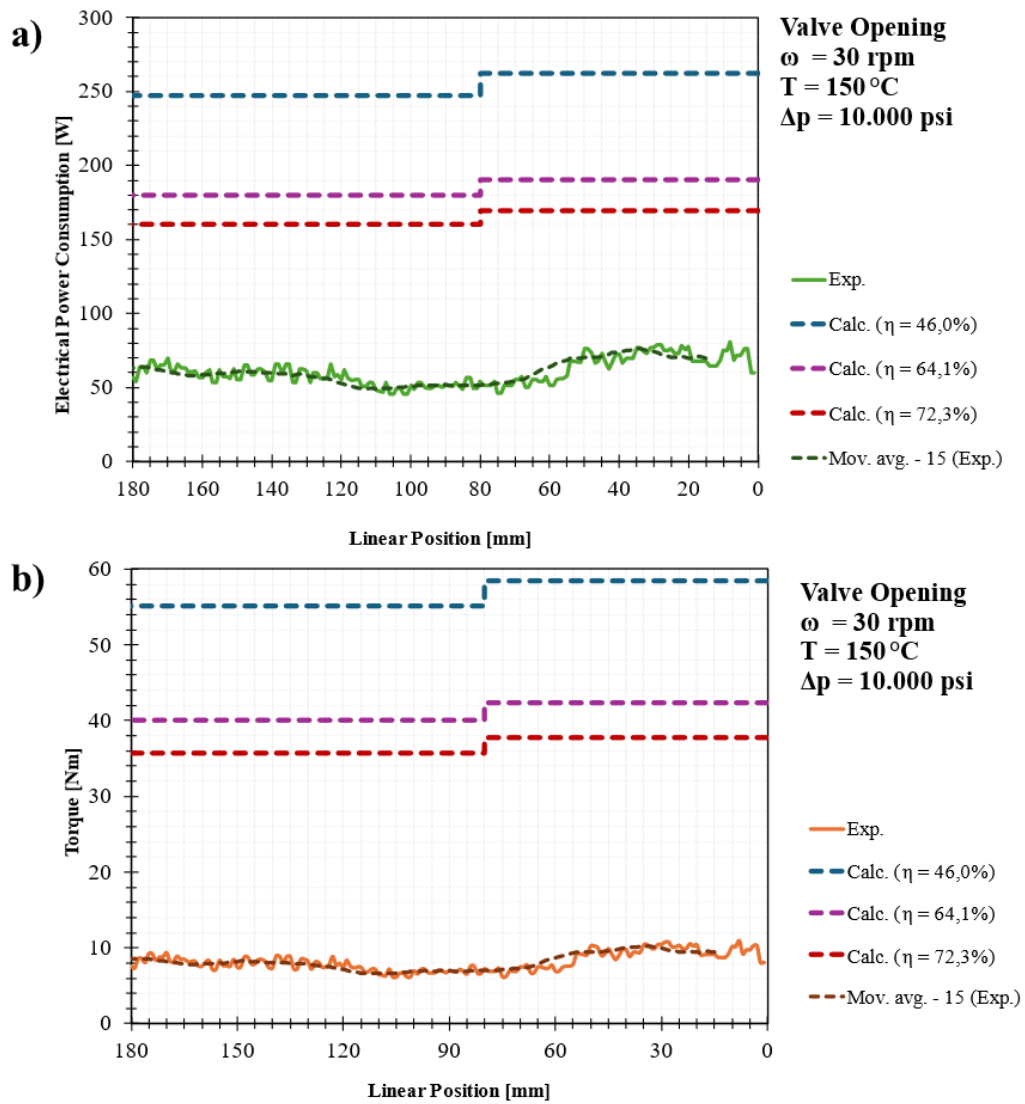
Figure 51: Comparison between calculated results and experimental data for the cycling test at 150 °C and 10.000 psi differential pressure for the opening movement of the sliding sleeve. a) Electrical power consumption versus linear position. b) Torque versus linear position (Author)

Figure 52: Comparison between calculated results and experimental data for the cycling test at 150 °C and 10.000 psi differential pressure for the closing movement of the sliding sleeve. a) Electrical power consumption versus linear position. b) Torque versus linear position (Author)
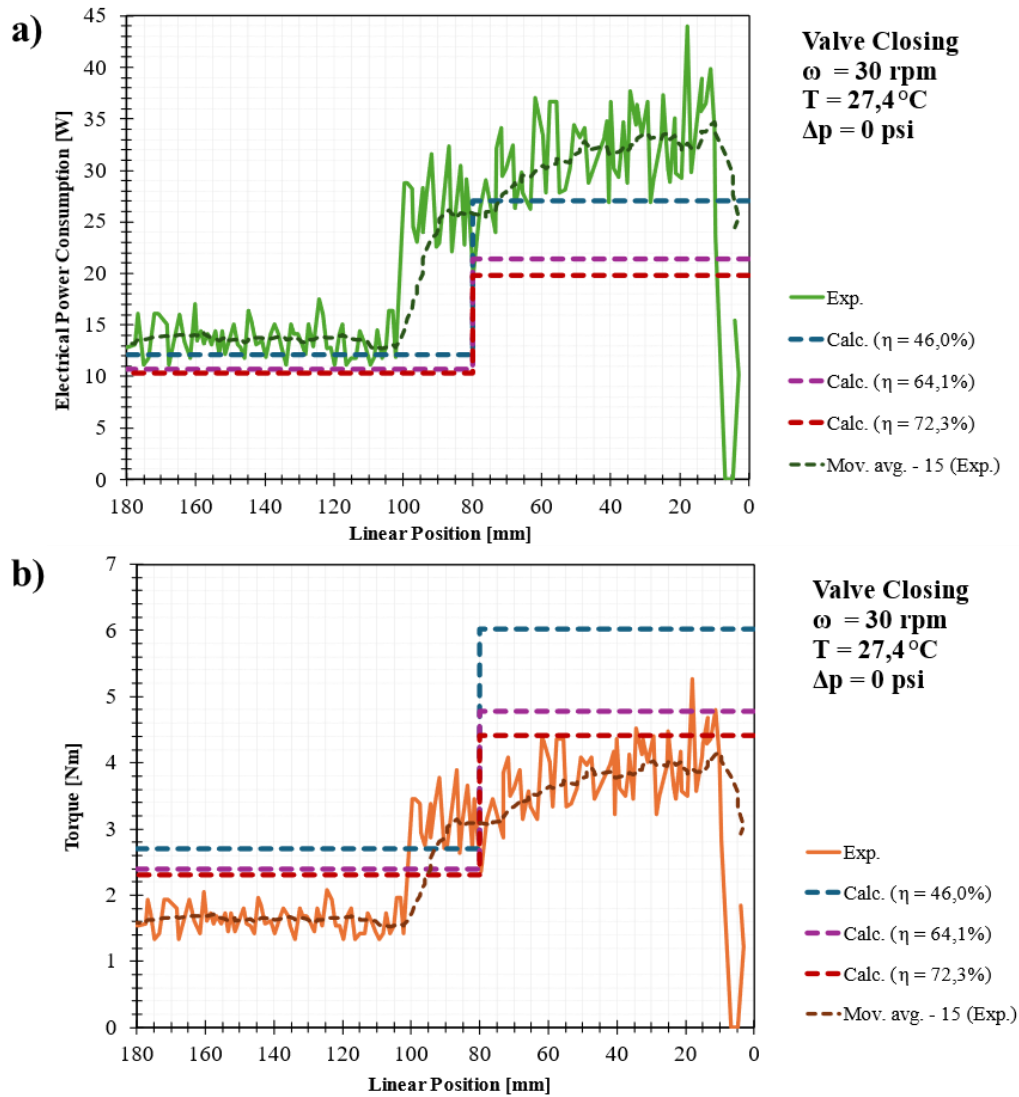
4.2.3

Differential Pressure Opening Test at Low and High Temperature

Figure 53 presents the comparison plots for the electrical power consumption (Figure 53a) and torque (Figure 53b) for the differential pressure opening test at 10°C .with 1.500 psi of differential pressure along the closing seal section and valve opening movement. Both plots show conservative results for all efficiencies from 0 to 80 mm (closing seal section) and, from 80 to 130 mm, as the differential pressure is zero, the results are fairly accurate for all three efficiencies. Figure 54 shows the analogous for the closing movement, where the results are close, but the empirical curves behavior are not so precise for both electric power consumption (Figure

54a). and torque (Figure 54b). During the closing movement, the differential pressure was zero.

Figure 53:Comparison between calculated results and experimental data for the differential pressure opening test at 10 °C and 1.500 psi differential pressure for the opening movement of the sliding sleeve. a) Electrical power consumption versus linear position. b) Torque versus linear position (Author)
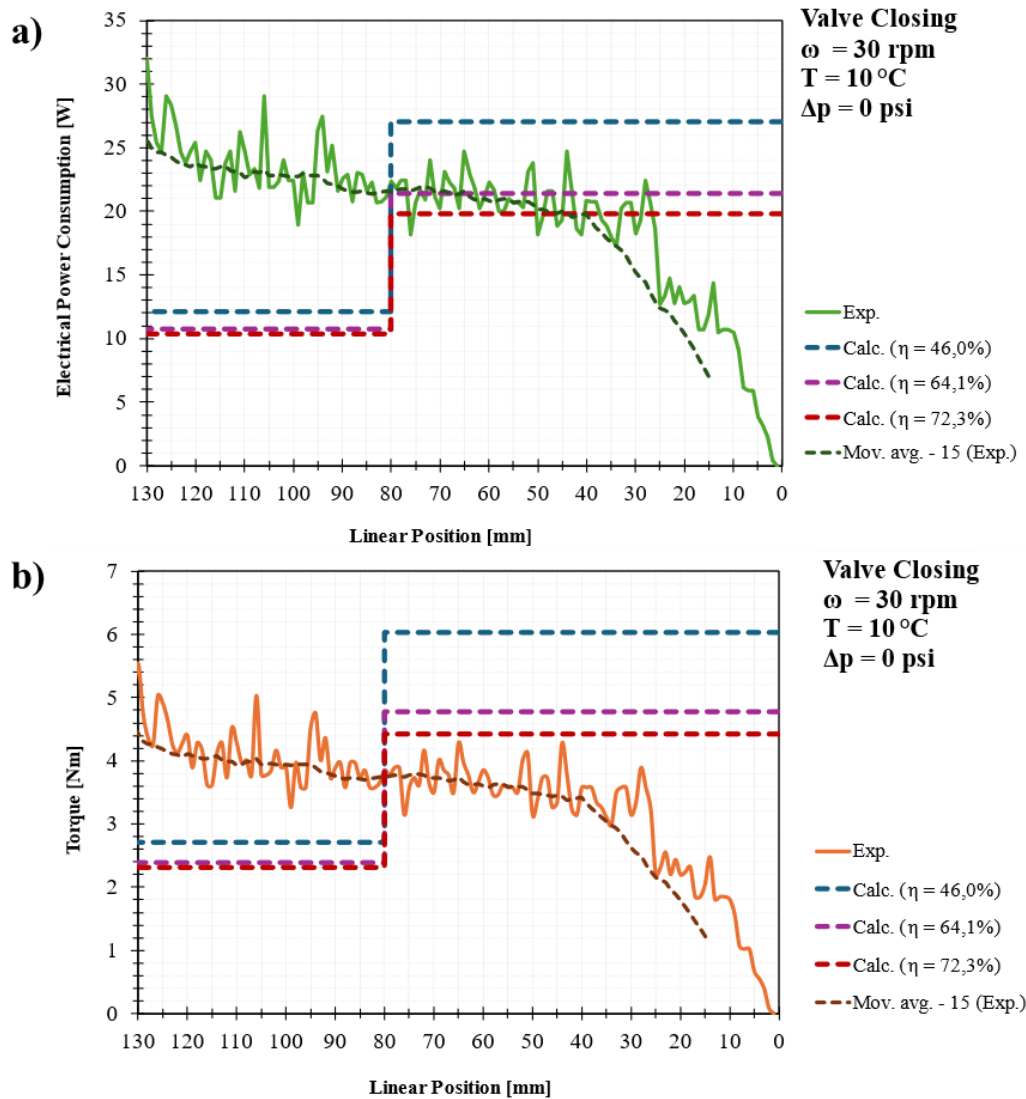
Figure 54: Comparison between calculated results and experimental data for the differential pressure opening test at 10 °C and 1.500 psi differential pressure for the closing movement of the sliding sleeve. a) Electrical power consumption versus linear position. b) Torque versus linear position (Author)
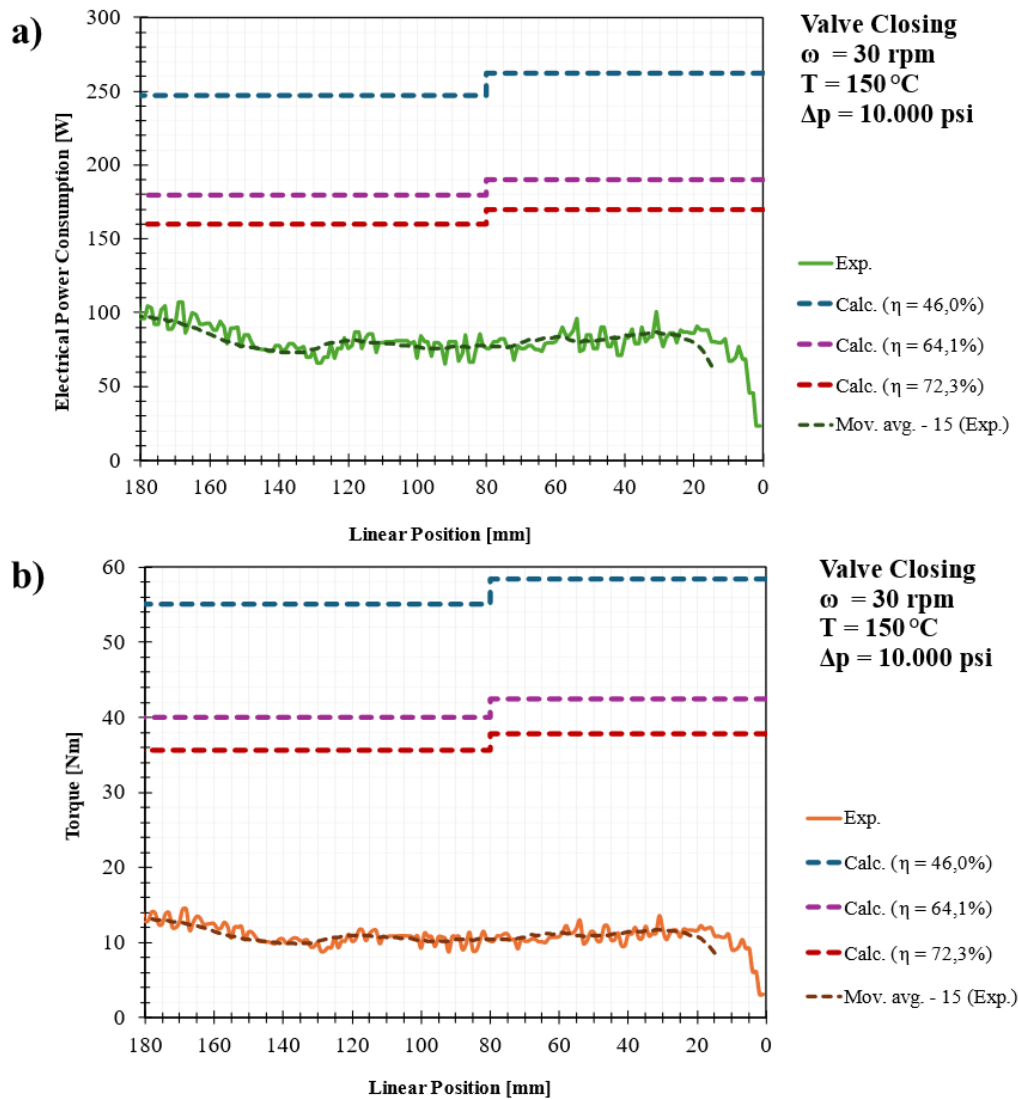
Similar to the previous evaluation, Figure 55 presents the comparison plots for the electrical power consumption (Figure 55a) and torque (Figure 55b) for the differential pressure opening test at 150°C .with 1.500 psi of differential pressure along the closing seal section and valve opening movement. The calculated results are conservative from 0 to 80 mm and slightly lower from 80 to 130 mm in the electrical power plot. For the torque plot, from 0 to 80 mm the theoretical are conservative and fairly precise from 80 to 130 mm. Figure 56, for the closing movement, has relative precise results for both electric power consumption (Figure 56a). and torque (Figure 56b) and the curve behavior follows the calculated ones.
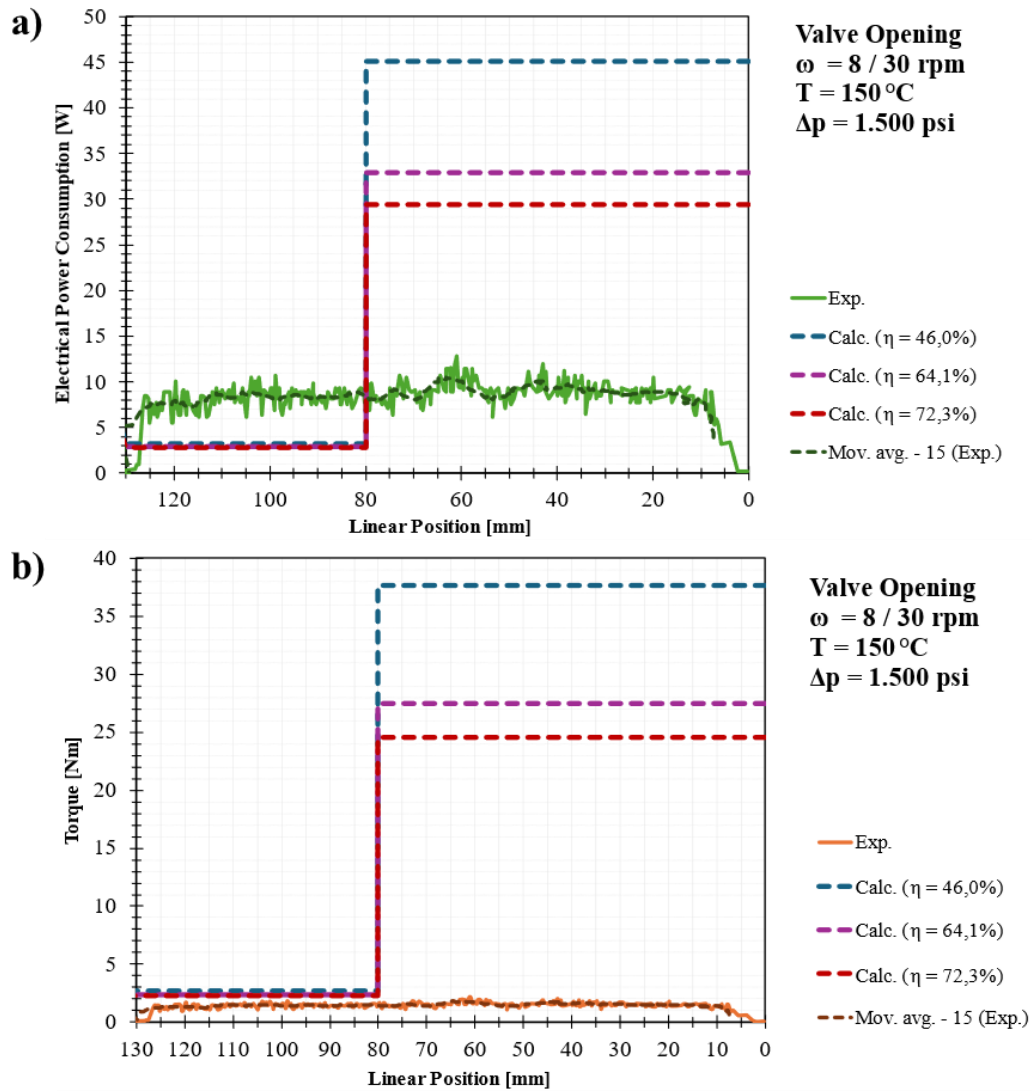
Figure 55: Comparison between calculated results and experimental data for the differential pressure opening test at 150 °C and 1.500 psi differential pressure for the opening movement of the sliding sleeve. a) Electrical power consumption versus linear position. b) Torque versus linear position (Author)
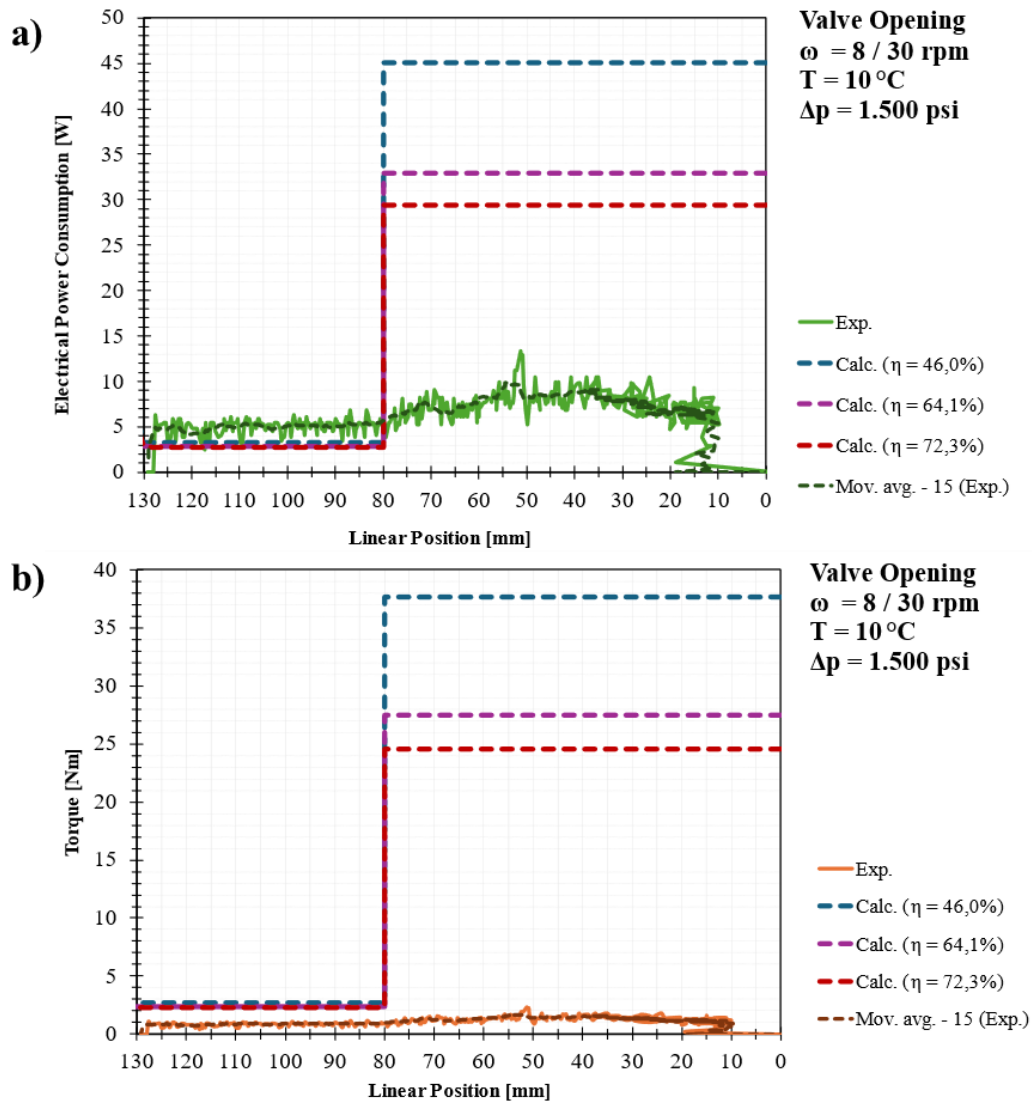
Figure 56: Comparison between calculated results and experimental data for the differential pressure opening test at 150 °C and 1.500 psi differential pressure for the closing movement of the sliding sleeve. a) Electrical power consumption versus linear position. b) Torque versus linear position (Author)
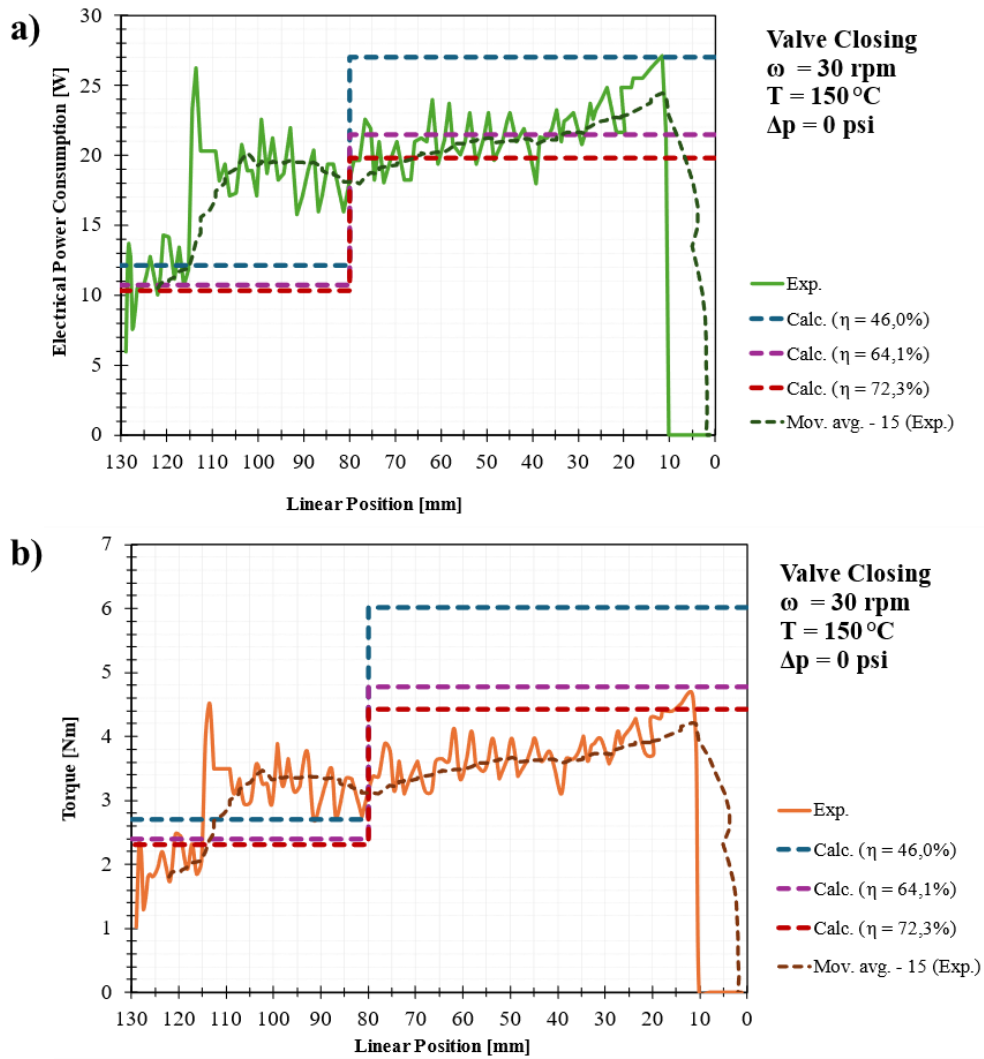
5
Conclusion

This dissertation investigated the design feasibility of an electromechanical actuator to be used in electric interval control valves (ICV), given the electrical power limitations of electric intelligent well completion (IWC) systems, through the adoption of a mathematical model. The validation was carried out via the comparison between the calculated results with the actual data from the physical tests in which the actuator was shifted at operational conditions of room temperature and zero differential pressure (functional test), 10.000 psi of pressure during the cycling test at 150 °C, 1.500 psi of differential pressure while opening the valve at 10 °C and 150 °C.

The key findings and contributions of this work are listed below:

1. The mathematical model successfully supported the electromechanical actuator's design, as the full-scale prototype was concept-proven achieving the TRL4;

2. Calculated results were accurate for the functional tests at room temperature and zero differential pressure during the closing movement of the Electric ICV;

3. Experimental results for the tests with differential pressure at high and low temperature showed the calculations for electrical power consumption and torque required were conservative in most cases;

4. Through the validation of the methodology used, the design of electromechanical actuators for different operational scenarios and valve dimensions can be done with the proposed mathematical model.

While the main purpose of this work was successfully achieved, some limitations of the model and further improvements for future works were identified and are presented below:

1. The differences between the calculation results and empirical data when differential pressure and high or low temperatures can be improved by a more detailed consideration of the mechanical interfaces temperature and wear influence for the friction torques and forces estimation;

2. The actual data from the viscous coefficient of friction and influencing factors of seal materials and geometries can provide more accurate results;

3. The scenario of scale deposition in the flow area of the ICV can be further studied to predict the increase of friction and power consumption through the tool's lifetime;

4. With adaptations for the fail-safe feature, the model can support the design of an electromechanical actuation system for a surface-controlled subsurface safety valve (SCSSV);

In conclusion, this research showed that the design feasibility analysis through the mathematical modelling of the electromechanical actuator was fitted for the proof of concept and laboratory validation (TRL 4) of the electric interval control valve (ICV) project, which this work was part of.

6
Bibliography

[1]   D. Zhu and K. Furui, Modern Completion Technology for Oil and Gas Wells, McGraw Hill Education, 2018.

[2]   H. W. Jr, Petroleum Engineering Handbook Volume VI: Emerging and Peripheral Technologies, Richardson: Society of Petroleum Engineers, 2007.

[3]   J. C. Rodriguez and A. R. Figueroa, "SPE 139404: Intelligent Completions and Horizontal Wells Increase Production and Reduce Free-Gas and Water in Mature Fields," in *SPE Latin American & Caribbean Petroleum Engineering Conference*, Lima, 2010.

[4]   SLB, "coning," SLB, [Online]. Available: https://glossary.slb.com/en/terms/c/coning. [Accessed 14 04 2024].

[5]   SLB, "Downhole Interval Control Valves (ICVs)," SLB, [Online]. Available: https://www.slb.com/products-and-services/innovating-in-oil-and-gas/completions/well-completions/intelligent-completions/downhole-interval-control-valves. [Accessed 12 04 2024].

[6]   J. Bellarby, Well Completion Design, Elsevier, 2009.

[7]   McKinsey & Company, "Technology Trends Outlook 2023," McKinsey Digital, 2023.

[8]   C. Beck, S. Rashidbeigi, Occo Roelofsen and E. Speelman, "The future is now: How oil and gas companies can decarbonize," McKinsey & Company, 7 January 2020. [Online]. Available: https://www.mckinsey.com/industries/oil-and-gas/our-insights/the-future-is-now-how-oil-and-gas-companies-can-decarbonize. [Accessed 20 March 2024].

[9]   IEA - International Energy Agency, "Emissions from Oil and Gas Operations in Net Zero Transitions," 2023.

[10] Oil & Gas Authority, "UKCS Energy Integration Final Report," Aberdeen, 2020.

[11] M. Potiani and M. Eduardo, "OTC-25391-MS: A Review of IC Installations: Lessons Learned from Electric-Hydraulic, Hydraulic and All-Electric System," in *Offshore Technology Conference*, Houston, 2014.

[12] S. Hiron and S. Edmundson, "Demystifying oil and gas electrification for today's energy transition," SLB, [Online]. Available: https://www.slb.com/resource-library/insights-articles/demystifying-oil-and-gas-electrification-for-todays-energy-transition. [Accessed 20 March 2024].

[13] J. Feder, "Subsea Electrification: Is the Tide About To Turn?," *Journal of Petroleum Technology 73,* pp. 26-29, 2021.

[14] B. Wright, "Plug-In Platforms: The Push for Offshore Electrification.," *Journal of Petroleum Technology 74,* pp. 36-44, 2022.

[15] R. MacKenzie, G.-R. Halvorsen and H. Vedeld, "OTC-305515-MS: Subsea All Electric – A Game Changing Technology Going Forward," in *Offshore Technology Conference*, Houston, 2020.

[16] P. H. Tee, H. V. Nguyen and W. I. Rinezry, "Partial Electrification of an FPSO Operating in the Brazilian Pre-Salt Region," in *Offshore Technology Conference*, Houston, 2023.

[17] MISC, "Offshore Business," MISC, [Online]. Available: https://www.miscgroup.com/our-solutions/offshore-business. [Accessed 11 04 2024].

[18] "ADVANCED GAS PATH UPGRADE FOR 9F GAS TURBINES," GE VERNOVA, [Online]. Available: https://www.gevernova.com/gas-power/services/gas-turbines/upgrades/advanced-gas-path-9f. [Accessed 11 Abril 2024].

[19] Petrobras, "Pré-Sal," Petrobras, [Online]. Available: https://petrobras.com.br/pre-sal. [Accessed 16 April 2024].

[20] Governo do Brasil, "Polígono do Pré-Sal," 08 January 2021. [Online]. Available: https://www.gov.br/anp/pt-br/assuntos/exploracao-e-producao-de-oleo-e-gas/dados-tecnicos/mapas-e-p/poligono-do-pre-sal. [Accessed 20 March 2024].

[21] O. M. Moreira, "SPE90472: Installation of the World's First All-Electric Intelligent Completion System in a Deepwater Well," in *SPE Annual Technical Conference and Exhibition*, Houston, 2004.

[22] D. N. Rodrigues, L. B. Minassa, R. S. Nunes and L. C. P. Costa, "OTC-28056-MS: Intelligent Completions as a Key Technology in Brazilian Presalt," in *Offshore Technology Conference Brasil*, Rio de Janeiro, 2017.

[23] E. Schnitzler, L. F. Gonçalez, R. S. Roman, D. A. S. d. S. Filho, M. Marques, R. C. Esquassante, N. J. Denadai, M. F. d. Silva, F. R. Gutterres and D. S. Gozzi, "SPE-195935-MS: 100th Intelligent Completion Installation: A Milestone in Brazilian Pre-Salt Development," in *PE Annual Technical Conference and Exhibition*, Calgary, 2019.

[24] R. N. A. M. Sawaguchi, F. G. Noel, F. C. G. Oliveira, A. M. B. Braga, M. A. S. Fernandes, D. S. Santos and F. Kirnbauer, "OTC-35415-MS: Development of an Electrically Actuated Inflow Control Valve for the Brazilian Pre-Salt Wells: A Reliability Approach, Challenges and Outcomes," in *Offshore Technology Conference 2024*, Houston, 2024.

[25] Oceaneering, "Subsea Distribution Products," Oceaneering, [Online]. Available: https://www.oceaneering.com/subsea-distribution-solutions/products/. [Accessed 15 April 2024].

[26] ouronova, "eSCM - Módulo de Controle Submarino Elétrico," ouronova, [Online]. Available: https://ouronova.com/escm-modulo-eletronico-de-controle-submarino/. [Accessed 16 April 2024].

[27] J. Wang, N. Zhang, Y. Wang, B. Zhang, Y. Wang and T. Liu, "Development of a downhole incharge inflow control valve in intelligent wells," *Journal of Natural Gas Science and Engineering,* pp. 559-569, 4 February 2016.

[28] O. B. Samuel, A. A. Chandrakant, F. A. Salleh, A. Jamil, Z. Ibrahim and A. Ivey, "SPE-202130-MS: All-Electric Intelligent Completion System: Evolution of Smart Completion," in *SPE/IADC Middle East Drilling Technology Conference and Exhibition*, Abu Dhabi, 2021.

[29] B. Bouldin, C. Verma, I. Bellaci, M. Black, S. Dyer, J. Algerøy, T. D. Oliveira and Y. Pan, "SPE-166507-PA: Prototype Test of an All-Electric Intelligent-Completion System for Extreme-Reservoir-Contact Wells," *SPE Drilling & Completion 29,* pp. 353-362, 16 September 2014.

[30] S. Jacob, I. J. Bellaci, P. Nazarenko and P. Joseph, "Designing, Planning and Installation of an 8-Zone All-Electric Intelligent Completion System in an Extreme Reservoir Contact Well," in *SPE Middle East Intelligent Oil and Gas Conference and Exhibition*, Abu Dhabi, 2015.

[31] American Petroleum Institute, "API 17Q: Recommended Practice on Subsea Equipment Qualification," API, Washington, 2017.

[32] W. M. Kimmel, P. M. Beauchamp, M. A. Frerking, T. R. Kline, K. K. Vassigh, D. E. Willard, M. A. Johnson and T. G. Trenkle, "Technology Readiness Assessment Best Practices Guide," NASA, 2020.

[33] M. F. D. Silva, C. C. Jacinto, C. Hernalsteens, M. Nobrega, M. D. Soares, E. Schnitzler and L. B. Nardi, "OTC-27983-MS: Cableless Intelligent Well Completion Development Based on Reliability," in *OTC Brasil*, Rio de Janeiro, 2017.

[34] E. Schnitzler, A. F. M. Oliveira, D. V. Ferreira, F. J. D. Salvo, L. C. M. d. Cruz, M. F. d. Silva, M. Marques, M. V. D. Ferreira and R. S. Roman, "OTC-

31894-MS: Full Open Hole Intelligent Completion: A Game Changer in Brazilian Pre-Salt," in *Offshore Technology Conference*, Houston, 2022.

[35] American Petroleum Institute, "API Specification 19ICV 1st Ed.: Interval Control Valves (ICV)," API, Washington, 2023.

[36] Schaeffler, "Friction and increases in temperature," Schaeffler, [Online]. Available: https://medias.schaeffler.com.br/pt/friction-and-increases-in-temperature#Friction%20and%20increases%20in%20temperature. [Accessed 19 May 2024].

[37] BSI ISO, "BS ISO 76:2006+A1:2017: Rolling bearings — Static load ratings," The British Standards Institution, London, 2017.

[38] James Walker, "Chevron®," James Walker, [Online]. Available: https://www.jameswalker.biz/our-solutions/our-products/hydraulic-products/piston-seals/chevron. [Accessed 24 05 2024].

[39] Parker Hannifin Corporation, "FlexiSeal®," in *PTFE Seals - Design Guide*, pp. 84 - 85.

[40] NSK, "Ball Screws," in *PRECISION MACHINE COMPONENTS*, NSK, 2020, pp. B1 - B614.

[41] ouronova inovações tecnológicas, "eICV Technical Reports," Rio de Janeiro, 2019.